

Advanced III–V nanowire growth toward large-scale integration

3

X. Dai¹, A. Olivier¹, C. Wilhelm¹, S.A. Dayeh², C. Soci¹

¹Nanyang Technological University, Singapore; ²University of California San Diego, CA, USA

Several elaborate reviews on the properties of III–V nanowires (NWs) already exist in the literature (Hyun, Zhang, & Lauhon, 2013; Joyce et al., 2011; Lapierre et al., 2013; Soci et al., 2010; Yan, Gargas, & Yang, 2009); here we focus on the specific issue of large-scale integration, which we believe is of paramount importance to enable transition from the initial research and development phase to practical implementation of these unique systems and devices. Selective-area growth of ordered, vertical nanowire arrays and 3D structure from patterned locations, and the corresponding functional devices, will be discussed.

3.1 Synthesis of III–V NWs

Bottom-up growth offers a great freedom in fundamental study of NWs with extremely small diameters, excellent surface morphology, complex structures, and controllable crystallographic structures, enabled by precise control of growth mechanisms and techniques.

3.1.1 Growth mechanisms

During the last two decades, the growth of III–V NWs has been extensively studied. Diverse growth mechanisms of these 1D materials have been proposed among the research community. For the sake of discussion, we will broadly categorize growth mechanisms into two groups: (1) the vapor-phase mechanisms, which encompass vapor–liquid–solid (VLS), vapor–solid–solid (VSS), vapor–solid (VS), oxide-assisted growth (OAG), and self-catalytic growth (SCG); and (2) the catalyst-free selective-area (SA) growth. These growth mechanisms will be reviewed in the following sections, with particular attention paid to the controversies regarding applicability of the different vapor-phase models.

All the vapor-phase mechanisms require a catalyst M for NW growth. As shown in the dotted inset of Figure 3.1(a), M can be composed of (1) a non-III metal alloying with a group-III element ($M_x\text{III}_y$) that characterizes a VLS growth, (2) a multigrain M for VSS, (3) an oxide for OAG, or (4) a III element for SCG. The major role of M is to lower the nucleation energy of a III–V layer at the seed/substrate interface, promoting growth of NWs.

The surface free energy at the seed/substrate interface determines the crystal growth direction of the NWs. III–V NWs can present pure cubic zinc blende (ZB), pure

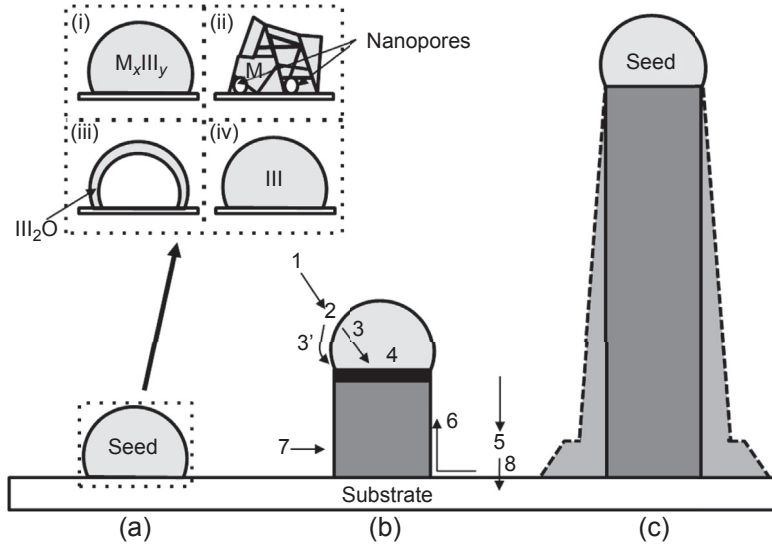








Figure 3.1 Scheme of NW growth mechanism process. (a) Formation of the seed with the different compositions (dotted inset): (i) alloyed M_xIII_y (VLS), (ii) multigrained (VSS) with possible nanopores (VQS), (iii) oxide-assisted III_2O or SiO_x (OAG), and (iv) III group element (SCG). (b) NW growth and the involved physical and chemical processes: (1) gas-phase diffusion, (2) dissociation reactions on the seed or on the NW surface, (3) diffusion of reactants through the seed or (3') along the seed to the seed/NW interface, (4) the formation of the semiconductor crystal at the liquid–solid interface (ledge) (Borgström, Verheijen, Immink, Smet, & Bakkers, 2006), (5) adsorption of precursor molecules on the substrate or NW surface, (6) surface diffusion, (7) crystal growth on the NW sidewall, and (8) film growth on the substrate surface. Steps 2, 4, 7, and 8 are activated processes, which depend exponentially on the temperature. (Adapted with permission from Verheijen, Immink, De Smet, Borgström, and Bakkers (2006). Copyright 2006, American Chemical Society.) (c) As-grown NW with straight or tapered (dashed lines) morphologies.

hexagonal wurtzite (WZ) or mixed crystal structures. For ZB NWs of relatively larger diameter, the preferred growth orientation is $\langle 111 \rangle$ due to the lower Gibbs free energy of nucleation for a $\langle 111 \rangle$ oriented NW with $\{110\}$ or $\{112\}$ facets (Schmidt, Senz, & Gösele, 2005) compared to $\langle 110 \rangle$ and $\langle 112 \rangle$ that are commonly observed at smaller diameters (particularly sub-20 nm diameters in Ge and Si (Dayeh & Picraux, 2010)). The $\{111\}$ substrate can possess either a cation (group-III) terminated surface known as (111)A or an anion (group-IV) terminated surface known as (111)B and the latter is more commonly used than the former in NW growth. In contrast to bulk arsenide and phosphide III–V materials, arsenide and phosphide NWs can crystallize in WZ orientation due to high levels of supersaturation and strong influence of NW facets on nucleation energies, where WZ facets have lower energies than those for ZB (Glas, Harmand, & Patriarche, 2007). Table 3.1 summarizes growth directions, types of substrates, growth mechanisms, and occurrence of crystallographic defects, such as stacking faults (SFs), twin planes, and polytypism (alternation of ZB and WZ segments) in binary III–V NWs reported in the literature.

Table 3.1 Commonly observed growth directions and cross-sections for some III–V NWs. The listed references are not exhaustive

Material	Growth direction	Growth substrate	Growth mechanism	CSG ^a	SF ^b	PT ^c	References
GaAs	$\langle 111 \rangle_B / [0001]$	GaAs(111)B	VLS, SA		Yes	Yes	Hiruma et al. (1995)
	$\langle 110 \rangle$	GaAs(001)	VLS		No	No	Fortuna et al. (2008), Ghosh, Kruse, and Lapierre (2009), and Mikkelsen, Sköld, Ouattara and Lundgren (2006)
	$\langle 110 \rangle$	GaAs(100)	VLS		No	No	Wu et al. (2003)
	$\langle 112 \rangle$		VLS				Givargizov (1975)
	$\langle 100 \rangle$	Si(111)	VLS		No	No	Ihn, Song, Kim, and Yong Lee (2006)
	$\langle 111 \rangle_A$	GaAs(111)A	VLS		No	No	Wacaser, Deppert, Karlsson, Samuelson, and Seifert (2006)
	InP	$\langle 111 \rangle_B / [0001]$		VLS		Yes	Yes
$\langle 110 \rangle$		InP(110)	SCG		No		Mattila, Hakkarainen, Jiang, Kauppinen, and Lipsanen (2007)
$\langle 100 \rangle$		InP(001)	VLS				Krishnamachari et al. (2004)
InAs	$\langle 111 \rangle_B / [0001]$	GaAs, InAs(111)B	VLS, SA		Yes	Yes	Hiruma et al. (1995)
	$\langle 100 \rangle$	InAs(001)	VLS, (VSS)				Seifert et al. (2004)
	$\langle 110 \rangle$	InAs(001)	VLS, (VSS)				Seifert et al. (2004)
	$\langle 112 \rangle$	InAs(111)B	VLS				Zhang, Zou et al. (2009)

Continued

Table 3.1 Continued

Material	Growth direction	Growth substrate	Growth mechanism	CSG ^a	SF ^b	PT ^c	References
GaP	$\langle 111 \rangle$ B		OAG		Yes	No	Liu et al. (2005)
	$\langle 111 \rangle$ B	Si(111)	VLS		Yes	No	Tateno, Hibino, Gotoh, and Nakano (2006)
GaSb	$\langle 110 \rangle$	Si(111)	OAG		Yes	No	Shi, Zheng, Wang, Lee, and Lee (2001)
	$\langle 111 \rangle$ B	GaAs(111)B	VLS		No	No	Jeppsson, Dick et al. (2008) and Jeppsson, Dick, Wagner et al. (2008)
	$\langle 110 \rangle$		VLS		No	No	Vaddiraju et al. (2007)
	$\langle 110 \rangle$		VLS		No	No	Pendyala et al. (2010)
InSb	$\langle 111 \rangle$ B	InSb(111)B	VLS			No	Gutsche et al. (2012) and Lugani et al. (2012)
	$\langle 220 \rangle$	InSb(111)B	VLS				Gutsche et al. (2012) and Lugani et al. (2012)
	$\langle 111 \rangle$	InSb(-1-1-1)B	VLS		Yes	No	Vogel, De Boor et al. (2011)
	$\langle 111 \rangle$	InP(111)B	VLS		No	No	Plissard et al. (2012)
	$\langle 110 \rangle$	InSb(111)	VLS		No	No	Park, Prokes, Twigg, Ding, and Wang (2007) and Paul et al. (2010)

^aCross-sectional geometry.^bStacking faults.^cPolytype.

Adapted with permission from Fortuna and Li (2010). Copyright 2010, IOP Publishing.

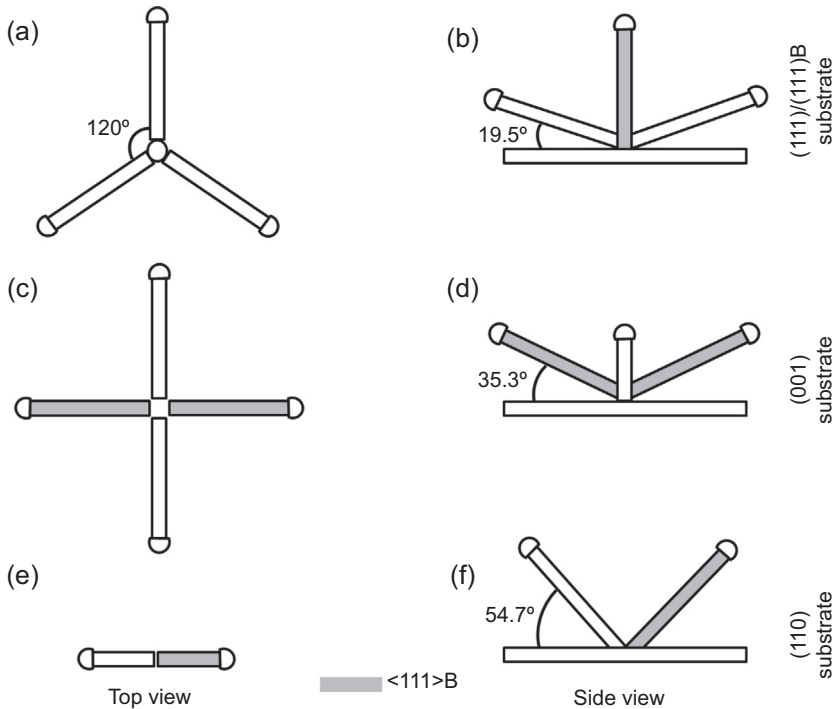


Figure 3.2 Schematic illustration of $\langle 111 \rangle$ NWs grown epitaxially on several substrates with different orientations. Both elemental and compound semiconductor substrates are combined into the same illustrations with $\langle 111 \rangle$ B direction specified via gray shading of the NW. Adapted with permission from Fortuna and Li (2010). Copyright 2010, IOP Publishing.

Figure 3.2 illustrates out-of-plane $\langle 111 \rangle$ growth direction on (111), (110), and (001) substrates, showing different angles relative to the substrates as well as various azimuth between NWs. NWs growing perpendicular to the substrate are only observed in Figure 3.2(a) and (b) with $\langle 111 \rangle$ B growth direction on (111)B substrate. Such growth is energetically favorable, which promises application of III–V NWs in vertically aligned NW array devices. On (001) substrate, NWs normally grow in four $\langle 111 \rangle$ directions with 90° between one another, as shown in Figure 3.2(c) and (d). Exceptionally, aligned planar $\langle 110 \rangle$ NWs grown on GaAs(001) substrate have also been achieved through the modulation of growth temperature (Fortuna, Wen, Chun, & Li, 2008). On (110) substrate, two $\langle 111 \rangle$ directions are azimuthally separated by 180° (Figure 3.2(e) and (f)).

VLS is the most common growth mechanism describing the NW growth. This model was first introduced to describe the growth of Si nanowhiskers (Wagner & Ellis, 1964), where the elongation of the Si nanowhiskers is driven by the continuous supersaturation inside the eutectic liquid seed by absorbing gaseous precursors. The diameter of these wires is mainly determined by the size of the catalysts. A handful of M can be used to mix with a single III element to form the right $M_x\text{III}_y$ alloy seed (Nguyen, Ng, & Meyyappan, 2005). The most common catalyst is Au, since it can form many stable eutectic alloys with the different III elements—for example, AuGa (Harmand

et al., 2005), AuIn (Lee, Wang, & Matijasevic, 1993). The shape, size, and composition of the alloy seed are determined by the growth conditions including the annealing temperature, the growth time, and the chamber environment (Harmand et al., 2005). Note that NWs can only grow when the temperature is above the alloy eutectic point in the VLS growth regime.

Below the eutectic temperature, the M_xIII_y alloy is not stable and VLS should not occur. However, many groups reported growths below the eutectic point (Persson, Larsson et al., 2004; Persson, Ohlsson, Jeppesen, & Samuelson, 2004), for example, GaAs and InAs with Au catalysts (Dick et al., 2005). With the help of X-ray energy-dispersive spectrometer and 3D model simulations (based on mass transfer and chemical reaction kinetics equations), Persson et al. demonstrated that in the absence of any growth precursors on a transmission electron microscope (TEM) heating stage, the catalyst stayed in solid-phase at temperatures that are comparable to the growth temperature of GaAs NWs and the growth was proposed to follow the VSS growth mechanism. Recent *in situ* TEM studies have shown that the bulk-phase diagram cannot be used to explain NW growth due to liquidus line suppression and lowering of the eutectic temperature (Sutter & Sutter, 2010). In addition, the presence of a low partial pressure of the input reactant can substantially lower the metal-reactant eutectic temperature by over 120 °C (Gamalski, Tersoff, Sharma, Ducati, & Hofmann, 2010), substantiating the universal applicability of the VLS mechanism at deep sub-eutectic temperatures. (Figure 3.1(a)(ii) and Figure 3.3(b)), based on solid-phase diffusion. In principle, the growth rate of VSS should be low for different reasons: (1) the diffusions of the III, V elements to the interface seed-substrate or seed-NW (i.e., the ledge, Figure 3.1(b)(3')) are very slow; and (2) the solubility of the V elements inside the seed is very low. It was estimated that the growth rate for VSS was 100 times lower in magnitude than for VLS (Kodambaka, Tersoff, Reuter, & Ross, 2007) accompanied with a significant taper (sidewall growth) of the NW. However, by comparing the growth rate for GaAs, InP, or InAs NWs under diverse growth mechanisms reported in the literature (Dayeh, Yu, & Wang, 2007d; Dick et al., 2005; Novotny & Yu, 2005; Persson, Fröberg, Jeppesen, Björk, & Samuelson, 2007; Tchernycheva et al., 2007) and summarized in Table III of Mohammad (2009), the growth rates under VSS and VLS are quite equivalent. As suggested by Mohammad et al., and despite the different proposed growth modes, the growth rates are similar. Mohammad postulated that the VSS growth of III–V NWs does not follow a standard VSS mechanism but a vapor–quasisolid–solid mechanism (VQS).

A solid alloy seed characterizes VQS with presence of semimolten nanopores (Figure 3.1(a)(ii)). The nanopores are formed by the transition phase (solid to liquid), lowering thus the activation energy by many parameters, that is, contaminants inside the chamber, inside the alloy seed, at the interface between the seed and the substrate or the seed and the NW, and the solubility of M in III (or vice-versa). Small diameter as-grown GaAs NW presents a solid Au tip (extremely low solubility of Ga in Au because of the Gibbs–Thomson effect (Givargizov, 1975)), while thicker NW exhibits an AuGa₂ alloy tip (Dayeh, Chen et al., 2008).

Instead of using a noble metal as a catalyst to induce the nucleation and the growth of the NWs, a semiconductor-oxide or metal-oxide can also be used to assist the

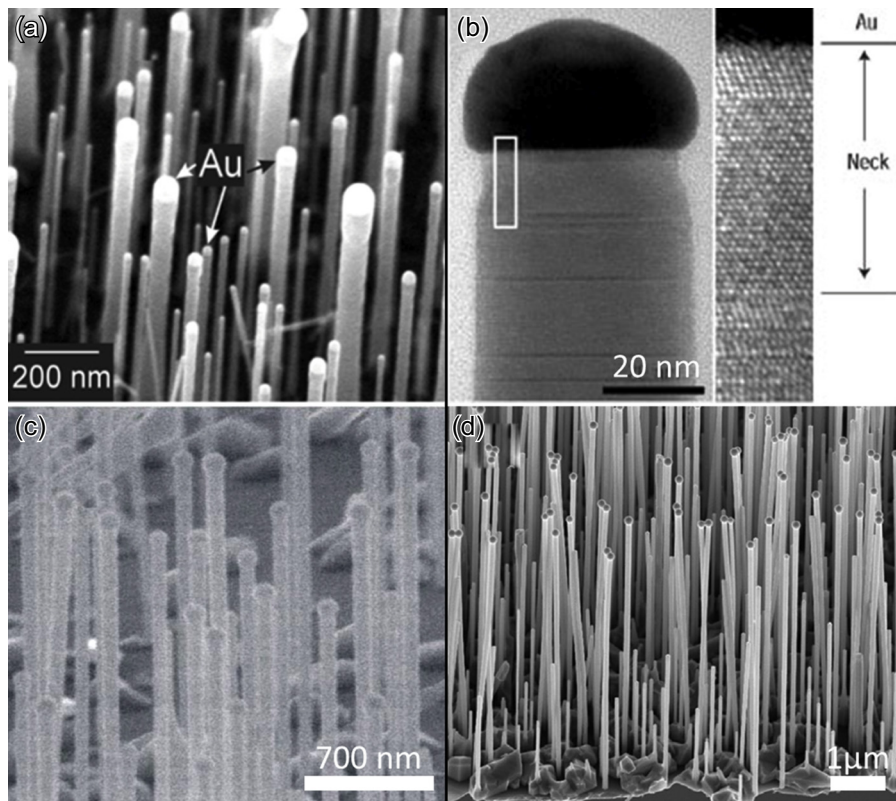
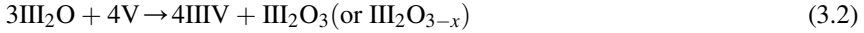


Figure 3.3 Electron microscope images of NWs grown by vapor-phase mechanisms. (a) InP NWs by VLS. (Reprinted with permission from [Bhunia, Kawamura, Fujikawa, Tokushima, and Watanabe \(2004\)](#). Copyright 2004 with permission from Elsevier.) (b) GaAs NWs by VSS. (Reprinted with permission from [Persson, Larsson et al. \(2004\)](#). Copyright 2004 Nature Publishing Group.) (c) GaP NWs by OAG. (Reprinted with permission from [Fontcuberta I Morral, Colombo, Abstreiter, Arbiol, and Morante \(2008\)](#). Copyright 2008 AIP Publishing LLC.) (d) InP NWs by SCG. (Reprinted with permission from [Dheeraj et al. \(2013\)](#). Copyright 2013, Elsevier.)

synthesis ([Figure 3.1\(a\)\(iii\)](#)). This OAG mechanism was first introduced by Zhang et al. to explain the growth of Si NWs through SiO₂-assisted vapor-phase reaction at high temperature ([Zhang, Lifshitz, & Lee, 2003](#)), which has a similar growth rate compared to the VLS mechanism. OAG is a process that can be also applied to grow InP NWs and nanotubes: a powder mixture of (InP:In₂O₃) is heated at a high temperature (~1150 °C) in a conventional tube furnace, which allows the formation of InP NWs/nanotubes at the cold part of the furnace (~500–600 °C). By tuning the ratio of In₂O₃ in the initial powder mixture, one can modify the ratio of nanotubes and nanowires synthesized, but also tune the morphological characteristics of such nanostructures ([Tang, Bando, Liu, & Golberg, 2003](#)). OAG is also reported for the synthesis of GaP NWs via a laser-ablated target of GaP and Ga₂O₃ ([Shi et al., 2001](#)),

InAs NWs, and GaAs (Fontcuberta I Morral, Colombo, et al., 2008) (Figure 3.3(c)) NWs via the assistance of a thin layer of SiO_x that assists in creation of steps on the substrate surface that lower the nucleation energy for NW growth by a group-III growth seed. For III–V NWs, the vapor transport process is accompanied by an oxidation–reduction process and can be described as follows:



The catalyst M (here as a metal-oxide III_2O_3) and the alloy seed (also an oxide III_2O) are not fully solid and are composed of semimolten nanopores, similar to the cases of VSS and VQS.

In addition, SCG can occur when group-III elements act as M (Figure 3.1(a)(iv)). Instead of introducing extrinsic catalysts, intrinsic group-III elements provided by the surface reconstruction of the III–V substrate via a pre-annealing step can assist the synthesis. For instance, Novotny et al. reported the SCG growth of InP NWs using metal organic chemical vapor deposition (MOCVD) with TmIn and PH_3 precursors under In-rich growth conditions (Figure 3.3(d)). Heterogeneous reactions and supersaturation in the liquid droplet led to nucleation of NW growth. By varying the growth conditions from In-rich to In-deficient conditions, the NW density and their taper was controlled (Novotny & Yu, 2005).

NWs grown on a substrate patterned with arrays of metal catalyst enable the precise control of diameters and lengths. Such ordered growth provides a way to characterize synergetic effect, which is a technological challenge for repeatability criterion. It was observed by Borgström et al. on GaP NWs grown by MOCVD (Borgstrom, Immink, Ketelaars, Algra, & Bakkerserik, 2007) that the growth rate increased with decreasing distance between NWs. This effect originates from the better decomposition of the precursors (i.e., TMGa) by an increase of the surface collection area when the wire–wire spacing is reaching an optimum value, which is a competition between the Gibbs–Thomson effect and surface diffusion-limited growth.

Catalysts exist in the growth mechanisms discussed above. Metal catalysts are widely used for VLS and VSS growths; however, they usually act as unintentional impurities and form deep-level traps inside the NWs, degrading their electrical and optical properties. Moreover, catalyst instabilities, for example, diffusion of catalyst along the NW, can induce defects on the NW or extra growth on NWs (nanotrees).

Alternatively, catalyst-free SA growth enables the NW growth in well-defined locations without introducing any extrinsic catalysts. This method relies on a patterned thin SiO_2 layer with small openings defined by the combination of e-beam lithography and wet (or dry) etching covering the III–V substrate (Figure 3.4(a) top). It was developed in the early 1960s for Si layer growth (Joyce & Baldrey, 1962) and then transferred to the growth of III–V micropillar arrays (Hamano, Hirayama, & Aoyagi, 1997; Motohisa, Noborisaka, Takeda, Inari, & Fukui, 2004; Motohisa, Takeda, Inari, Noborisaka, & Fukui, 2004). Several groups investigated the role of the different growth parameters in the SA technique. Hamano et al. observed the growth rate

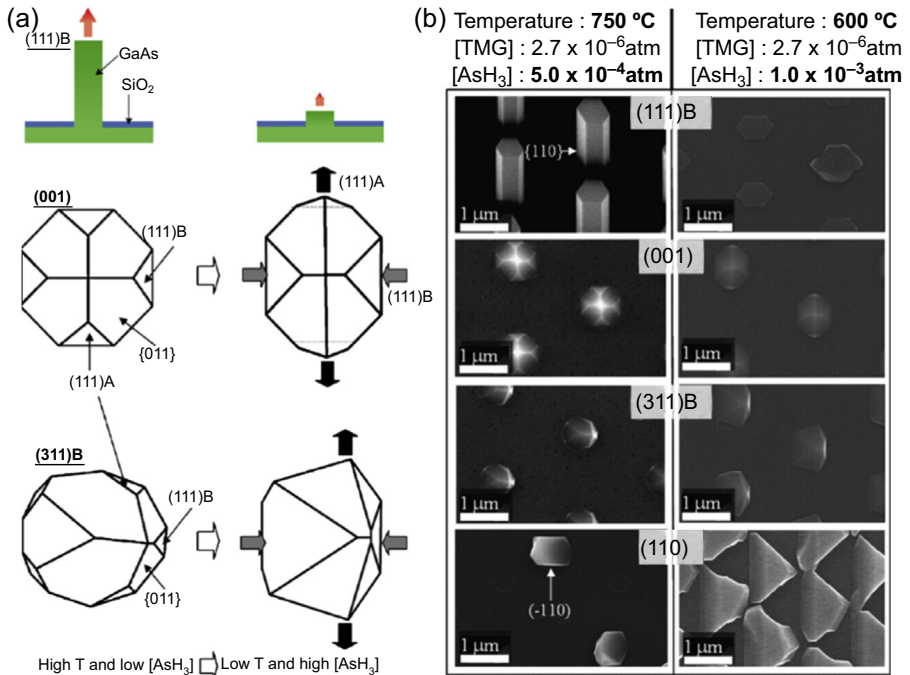


Figure 3.4 (a) Schematics of grown structures on (111)B, (001), and (311)B under growth condition A (high T_G and low $[\text{AsH}_3]$ (flow rate) condition, left) and B (low T_G and high $[\text{AsH}_3]$ condition, right). (b) Tilted and top view of SEM images of GaAs grown on (111)B, (001), (311) B, and (110) substrates. The images in the left column summarize the structure grown under high T_G and low $[\text{AsH}_3]$ condition, while those in the right column stand for the growth under low T_G and high $[\text{AsH}_3]$ condition.

Reprinted with permission from [Ikejiri et al. \(2007\)](#). Copyright 2007 with permission from Elsevier.

increased as the radius decreased and the GaAs micropillars with a hexagonal cross-section with smooth (-110) facets were formed during the growth on (111)B GaAs substrate. Ikejiri et al. reported an advanced study of GaAs NW growth on substrates with different orientations and growth conditions ([Ikejiri, Noborisaka, Hara, Motohisa, & Fukui, 2007](#); [Ikejiri et al., 2008](#)). As-grown GaAs NWs exhibited low index facets, and their growth rate was mainly determined by the growth parameters ([Figure 3.4](#)), that is, flow rate of AsH_3 , growth temperature and substrate crystal orientation.

It is of great importance to integrate NWs into the existing Si-technology platform in order to implement devices with novel functionalities. Despite the controversies about the vapor phase mechanisms, that is, the seed nature, VLS-grown vertical NWs are shown to be the best candidates for their integration in an Si platform.

3.1.2 Growth apparatus

Numerous growth methods have been developed to grow semiconductor-based thin films, and each method is dedicated to a specific application (e.g., light-emitting diodes

with MOCVD or quantum cascade lasers with molecular beam epitaxy (MBE)). Various techniques are also implemented in III–V NW growth: highly controllable methods including MOCVD, MBE, chemical beam epitaxy (CBE); and less controllable techniques such as chemical vapor deposition (CVD), laser-assisted catalytic growth (LCG), pulse laser ablation, and wafer annealing.

The first NW growth was realized on Si in 1964, where Si whiskers were grown on a halide saturating system (Theuerer, 1961) through the H₂ reduction of silicon tetrachloride (SiCl₄) precursor via the VLS mechanism (Wagner & Ellis, 1964), while the first III–V NW with well-understood growth mechanism was reported in the late 1990s. Hamano et al. selectively grew GaAs pillars with a submicron diameter using MOCVD (Hamano et al., 1997). In the late 1990s and early 2000s, NWs started to arouse interests and were extensively developed. Lieber et al. reported the growth of Si and Ge NWs through laser ablation and the VLS mechanism (Morales & Lieber, 1998). This technique consists of the pulsed laser ablation of a target containing the NW elements and the metal catalyst, followed by the condensation of the vapors into nanometer-sized clusters and NW growth via VLS. This technique was also implemented in the growth of III–V systems, for example, GaAs NWs (Duan, Wang, & Lieber, 2000), InP NWs (Duan et al., 2001; Gudiksen, Wang, & Lieber, 2001; Wang, Gudiksen, Duan, Cui, & Lieber, 2001), and GaAs/GaP heterostructure NWs (Gudiksen, Lauhon, Wang, Smith, & Lieber, 2002). However, it is limited by the availability of target sources and the absence of control of the NW position on the substrate.

MOCVD, also known as organic metallic vapor phase epitaxy (OMVPE) or MOVPE, is a growth process allowing the synthesis of single, polycrystalline, or amorphous material layers. The liquid precursors are metal-organic compounds, for example, trimethyl indium ((CH₃)₃In, TMIIn), tertiarybutyl arsine (TBAs), etc. (Figure 3.5(a)). After being introduced into the chamber, the precursors are decomposed through pyrolysis, enabling III and V atomic elements to bond to the surface of the heated substrate and form an epitaxial crystalline layer. This method was first developed in the late 1960s (Manasevit, 1968), though MOCVD-like fragments were patented in the early 1960s (Miederer, Ziegler, & Dotzer, 1962, 1963). MOCVD is considered as the most versatile, robust technique to grow various kinds of semiconductor materials (III–V, II–VI), with an excellent uniformity on a large scale and a high growth rate. The capability of forming an abrupt interface and selective epitaxial growth has made MOCVD one of the most appreciated and economical techniques for diverse industrial applications like LEDs, injection lasers (near IR-blue), solar cells, high-speed transistors, and photonic integrated circuits. It is of great importance to note that the quality of growth strongly depends on the growth conditions. Investigations have been made from homoepitaxy (i.e., on lattice-matched substrate) to heteroepitaxy (i.e., on Si substrates) (Mårtensson et al., 2004; Tateno et al., 2006; Tateno, Zhang, & Nakano, 2008); from axial (Björk et al., 2002; Borgström et al., 2006; Jeppsson, Dick et al., 2008; Svensson et al., 2005; Panev, Persson, Skold, & Samuelson, 2003) to radial NW heterostructures (Ganjipour, Ek et al., 2012; Lin et al., 2003; Mohan, Motohisa, & Fukui, 2006; Noborisaka, Motohisa, Hara, & Fukui, 2005; Tilburg et al., 2010); and with metal catalyst (Duan et al., 2001; Nilsson et al., 2009; Shi et al., 2001; Vaddiraju et al., 2007;

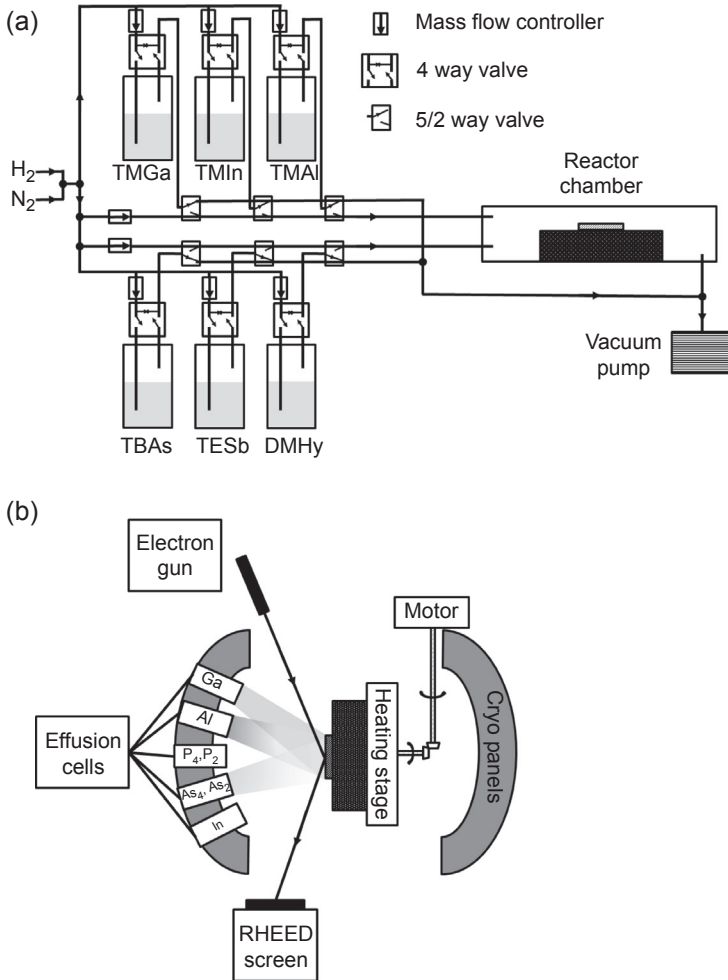


Figure 3.5 Scheme of (a) MOCVD A 5/2 way valve has 5 ports equally spaced and 2 flow positions. It can isolate and simultaneously bypass a passage way for the fluid which for example should retract or extend a double acting cylinder. A 4 way valve has four ports equally spaced round the valve chamber. The plug has two passages to connect adjacent ports. It can be used to isolate and to simultaneously bypass a sampling cylinder installed on a pressurized water line and (b) MBE setup.

Wu et al., 2003) and catalyst-free SA (Hamano et al., 1997; Motohisa, Noborisaka et al., 2004; Poole, Lefebvre, & Fraser, 2003) growth methods.

MBE is another growth method that allows the epitaxial growth of high-purity material and offers an abrupt interface between epi-layers in complex structures, promoting the development of device physics. It is a low-growth-rate technique based on the evaporation of solid (elemental) sources onto a heated substrate under ultra-high vacuum (UHV) conditions (Figure 3.5(b)). Because metal-assisted III–V NW growth is

very sensitive to the surface preparation (Fortuna & Li, 2010), an M source can be set up on the MBE to avoid contaminants from the M colloidal nanoparticle solution (Harmand et al., 2005). The high costs of precursors and system maintenance are the main drawbacks of this technique, responsible of the variation of process reproducibility. In addition, MBE is less versatile compared to MOCVD in terms of certain ternary and quaternary III-N materials growth due to the high vapor pressure of nitrides.

A hybrid technique combining features of MOCVD and MBE called chemical beam epitaxy (CBE) or metal organic MBE (MOMBE) was developed in the early 1980s (Veuhoff, Pletschen, Balk, & Lüth, 1981). In this case, the idea was to grow materials at UHV with metal-organic precursors. This system can use both solid and organometallic sources, but CBE also encountered similar issues as in MBE and MOCVD, the difficulty in growing nitride-based materials and the low throughput, hindering a widespread usage in the industry. Samuelson's group exploited III-V NW growth by CBE intensively on GaAs NWs (Persson, Larsson et al., 2004; Persson, Ohlsson et al., 2004), GaAs NW embedded with InAs quantum dots (Panev et al., 2003), and InAs NWs (Thelander et al., 2004). Growth of phosphide-based (Poole et al., 2003) and antimonide-based (Ercolani et al., 2009; Vogel, Boor et al., 2011; Vogel, De Boor et al., 2011) NWs was also reported.

3.2 Crystallographic properties

Progress in the bottom-up III-V NW synthesis has allowed the precise control of the crystalline structure, doping, heterostructure formation, and heteroepitaxial growth on Si, enabling the design of functional devices and their integration into a mainstream technology platform.

3.2.1 Crystallographic defects

Crystalline structure, as well as the occurrences of random structural defects and polytypism, can be precisely controlled during NW synthesis. While vacancy, anti-site, and interstitial defects are widely investigated in an III-N nanoscale system (Wang, Li, Gao, & Weber, 2010), twin boundaries (TBs) and SFs are usually considered in III-V nanostructures as main source of defects that can degrade device performance. For example, these defects can induce a variation of charge carrier concentration and an increment of phonon scattering (Schroer & Petta, 2010).

III-V NWs commonly exhibit a mixture of ZB cubic structure and wurtzite (WZ) hexagonal structure in the $\langle 111 \rangle$ direction (Algra et al., 2008; Caroff et al., 2008; Dayeh, 2010; Dayeh, Soci, Bao, & Wang, 2009; Dick, Caroff et al., 2010; Koguchi, Kakibayashi, Yazawa, Hiruma, & Katsuyama, 1992; Xiong, Wang, & Eklund, 2006), while their bulk counterparts usually crystallize in ZB. The ZB structure includes the stacking of monoatomic layers in the sequence of ...cAaBbCcA... in the $\langle 111 \rangle$ direction (Figure 3.6), whereas the WZ crystalline phase displays a stacking sequence of ...bAaBbA... in the $\langle 0001 \rangle$ direction. Due to the small difference in the cohesive energy of these two structures ($\Delta_{ZB-WZ} \leq 25$ meV) (Akiyama, Sano,

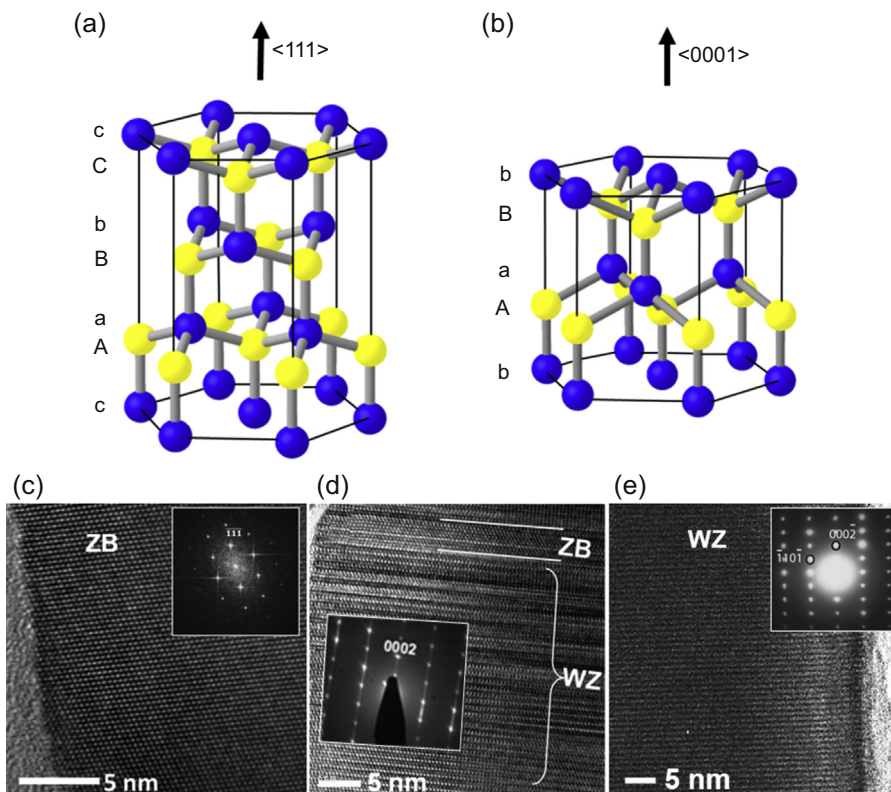


Figure 3.6 Polymorphism in III–V NWs. Ball-and-stick model of (a) the ZB structure in the $\langle 111 \rangle$ growth direction, showing the sequence of monoatomic stacking planes ...cAaBbCc... and (b) the WZ structure in the $\langle 0001 \rangle$ growth direction with stacking plane sequence ...bAaBb... (c–e) High resolution TEM images of (c) GaAs NW grown on GaAs (111)B surface. The electron diffraction pattern in the inset shows a pure ZB phase. (d) GaAs NW grown on Si (111) exhibiting a mixture of ZB and WZ phases. (Reprinted from Dayeh, Soci et al. (2009), with permission from Elsevier.) (e) SF free GaAs NW displaying pure WZ phase. (Reprinted with permission from Hoang et al. (2009). Copyright 2009, AIP Publishing LLC. Reproduced from Wilhelm et al. (2012), reproduced with permission of The Royal Society of Chemistry.)

(Nakamura, & Ito, 2006; Glas, Harmand, & Patriarche, 2007), polytypism is observed by the appearance of small segments of ZB in WZ when an SF misplaces an “Aa” plane with a “Cc” plane, or small WZ segments appearing in ZB after the introduction of two sequential twin planes, or a twin plane between which the ZB segment rotates 60° around the $\langle 111 \rangle$ axis from the original ZB structure (Caroff, Bolinsson, & Johansson, 2011; Caroff et al., 2008; Tomioka, Motohisa, Hara, & Fukui, 2007). Other than these, a 20–40 nm long 4H polytype (...bAaBbCcBbA...) was observed right above the inserted ZB GaAsSb segment in the WZ GaAs NW (Dheeraj et al., 2008), and a six-monolayer superlattice consisted of twinned and ZB structure was

also reported as a new stacking sequence (...cAaBbCcBbAaCcA...) (Mariager et al., 2007). Dayeh et al. found that the gradual multiplication of SFs in the region between two edge defects were caused by edge-nucleated defects-induced steps at the liquid–solid interface, which is a distinctive defect multiplication mechanism in layer-by-layer NW growth (Dayeh et al., 2012).

In general, the defecting segments within the primary structure are nucleating at the triple-phase contact line on the small side facets or defects, acting as a form of stored surface and interface energy release (Johansson et al., 2006; Joyce et al., 2008). Notably, both the interface energies at the triple-phase boundary and the supersaturation of the liquid seed significantly affect the nucleation process and consequently determine the definitive crystallographic phase (Glas et al., 2007; Wilhelm, Larrue, Dai, Migas, & Soci, 2012). Therefore, the preferential growth of a particular phase can be controlled by tuning relevant VLS growth parameters such as the V/III ratio, the temperature, and the NW radius. It is generally accepted that high supersaturation (i.e., with high growth temperature, low V/III ratio, and small radii) promotes the appearance of a WZ crystalline phase (Dubrovskii & Sibirev, 2008; Dubrovskii, Sibirev, Harmand, & Glas, 2008; Glas et al., 2007; Glas, Patriarche, & Harmand, 2010). The fraction of WZ phases in InAs NWs was reported to increase with decreasing the growth temperature (Caroff et al., 2008; Johansson et al., 2010).

3.2.2 Doping

Controllable doping in III–V semiconductor NWs is critical in the broad range of applications, including electronics (Duan et al., 2001; Thelander et al., 2006), photonics (Yan et al., 2009), optoelectronics (Cirlin et al., 2009; Colombo, Heibeta, Gratzel, & Fontcuberta i Morral, 2009), and quantum transport devices (Riel et al., 2012; Tomioka & Fukui, 2011; Wallentin et al., 2010). To modulate the electrical (i.e., carrier concentration, band gap energy, mobility, etc.) and optical properties (i.e., absorption coefficient, dielectric constant, etc.) of NWs, it is of great importance to understand the dopant incorporation mechanism during the growth, and its influence on crystalline structure and composition characterization methods.

NW doping can be achieved by either *ex situ* or *in situ* doping methods. *Ex situ* doping methods include monolayer doping, where the surface covalently bonded dopant monolayers are annealed and diffused into the sample (Ho et al., 2009); gas-phase doping by annealing NW in the dopant ambient (Ford et al., 2010); solid-state diffusion through predeposition and drive in of spin-on-dopant (Ingle et al., 2008); and ion beam implantation, which allows doping concentrations beyond the equilibrium solubility limit (Borschel et al., 2011). On the other hand, the *in situ* doping can be done via the particle-seeded growth by the inclusion of dopant precursor, which mainly contains two mechanisms. The major one contains dopant incorporation from the liquid catalyst droplet to the NW core by VLS, as illustrated in Figure 3.7(a). The doping efficiency is limited by the dopant concentration in the liquid catalyst and the solubility in the solid III–V NW. Otherwise, dopants are incorporated from the sidewall in the vapor-phase-epitaxy (VPE) mode, consisting of dopant absorption, diffusion, and desorption as indicated by a dashed arrow in Figure 3.7(b)

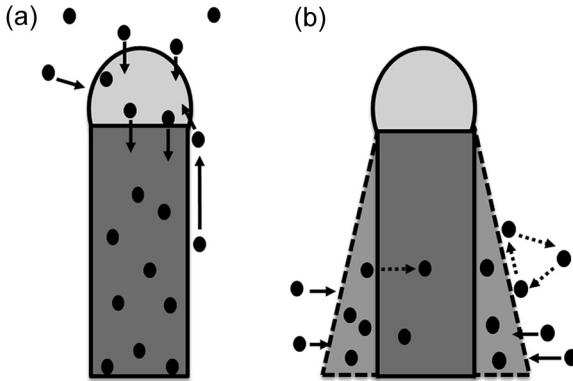


Figure 3.7 (a) Schematic diagram of dopant incorporation pathways via the VLS mode, where the dopants incorporate into the liquid catalyst, leading to a uniform doping concentration in the whole NW. (b) Schematic diagram of doping pathways via VPE mode comprising steps of dopants adsorption, migration, incorporation, and desorption on the sidewall of the NW.

(Casadei et al., 2013; Dufouleur et al., 2010; Schwalbach & Voorhees, 2009; Zhang, Tateno, Suzuki, Gotoh, & Sogawa, 2011).

Techniques such as hall measurement and secondary ion mass spectroscopy (SIMS) are widely used for determining the dopant incorporation and concentration in thin films. However, it is extremely challenging to adapt them into the characterization of an NW, high aspect ratio, one-dimensional system. Instead, some other methods are proposed to study the dopant distribution and *in situ* doping process.

Dopant concentration and carrier density are conventionally determined by electrical measurements, which includes resistivity mapping (Dheeraj et al., 2013; Dufouleur et al., 2010), field effect transistor (FET) characterization (Dayeh et al., 2007a; Rolland, Caroff, Coion, Wallart, & Leturcq, 2013; Thelander et al., 2010; Zhang et al., 2011), and capacitance–voltage (CV) measurement (Roddaro et al., 2008). The difference and repeatability in doping concentration can be compared by a qualitative measurement of the resistivity between multicontacts or different NWs. On the other hand, a quantitative estimate of doping concentration and mobility can be extracted from the linear regime of the FET I – V characteristics. The free carrier concentration at flat-band conditions, usually referred to as the electrically active dopant concentration, $n = (\rho e \mu)^{-1}$, where $\rho = RS/l$ is the resistivity, R is the NW resistance, S is the cross-sectional area, l is the contact separation, and μ is the field-effect mobility. The latter can be evaluated by $\mu = g_m L^2 / C_g V_d$, where $g_m = (dI_d/dV_g)_{\max}$ is the transconductance, L is the channel length, C_g is the gate capacitance. For a circular cross-section, $C_g = 2\pi\epsilon\epsilon_0 L / \ln(2t_{ox}/r)$, and for hexagonal-shaped NW,

$$C_g = \alpha(2\pi\epsilon\epsilon_0 L) / \cos h^{-1} \left(\left(t_{ox} + \frac{\sqrt{3}}{2} r^* \right) / r^* \right), \text{ with } r^* = 0.84r \text{ (Wunnicke, 2006).}$$

Using this method, Rolland et al. (Rolland et al., 2013) and Thelander et al. (Thelander et al., 2010) found that Si dopant primarily incorporated in the sidewall by radial overgrowth in case of Au-catalyzed InAs NWs grown in MBE and CBE, while

Zhang et al. (Zhang et al., 2011) demonstrated Si dopant to be predominantly incorporated in the core of the InAs wire through Au catalyst in MOCVD growth. The other method, CV characterization, allows quantifying the NW carrier concentration through an adapted radial metal-insulator-semiconductor FET (MISFET) model (Astromskas et al., 2010) and is more precise due to the direct measure of the gate capacitance without the use of assumptions relevant to parasitic capacitances and actual geometric gate capacitance.

Raman spectroscopy was reported to analyze the Si *in situ* doping mechanism, existence, concentration, and crystalline structure in the Ga-catalyzed GaAs NW grown by MBE (Dufouleur et al., 2010; Ketterer, Uccelli, & Morral, 2012). Si and Ge are amphoteric in III–Vs, which could result in either n-type or p-type doping and can be distinguished using Raman spectroscopy. The transverse optical (TO) and longitudinal (LO) phonon modes of GaAs can be identified at wavenumbers 263 and 288 per centimeter, while the lower density peaks at 384 and 393 per centimeter are attributed to local vibrational mode (LVM) of Si atoms on Ga sites (n-type) and As (p-type) sites, respectively. The position of LVM mode at 393 per centimeter and the increasing LVM to modes ratio from the tip to the base along the NW revealed a p-type behavior with higher doping concentration at the base of the GaAs NW, implying the possibility of dopant incorporation through the side facets.

Sophisticated tools like the atom probe tomography (APT) (Müller, Panitz, & McLane, 1968) performed on a local electrode atom probe (LEAP) microscope can be used to do the 3D atomic-resolution composition mapping of an NW from the sequential field evaporation of individual ions from the NW tip. Lauhon's group mapped the position of single Au atoms in an MOCVD grown InAs NW and found the interface between the $\text{Au}_{0.9}\text{In}_{0.1}$ catalyst and the InAs NW is extremely abrupt (less than 0.5 nm) (Perea et al., 2006). Sequentially, Du et al. demonstrated the elemental mapping of an Si-doped GaAs NW, where the distribution of Si dopants, carbon, hydrogen, and oxygen contaminations were measured and reconstructed into a 3D graph (Du et al., 2013).

Scanning tunneling microscopy (STM) is an alternative technique, being able to detect the quantitative information down to atomic precision (e.g., facet morphology, atomic structure, and surface composition characterization) (Bolinson et al., 2009; Mikkelsen, Skold et al., 2004; Xu et al., 2012). It has been used to detect the composition and diffusion of Sb in InAs/InAs_{1-x}Sb_x NW (Xu et al., 2012) and Mn in Ga_{1-x}Mn_xAs/GaAs superlattices (Mikkelsen, Ouattara et al., 2004).

In the meantime, other techniques such as out-of-plane X-ray diffraction and imaging (Davydok et al., 2013), X-ray energy-dispersive spectroscopy (XEDS) (Xu et al., 2012; Yang et al., 2013), electron energy loss spectroscopy (EELS) (Yang et al., 2013), and photoemission electron microscopy (Hjort et al., 2011) are also used to identify and map dopant incorporation in NWs.

3.2.3 Homo- and heterojunction formation

Compared to other nanostructure topologies, NWs have a unique degree of freedom to design nanoscale homo-/heterojunctions or to form monolithic junctions. Numerous physical phenomena arising from such low-dimensional nanostructures with large

surface-to volume ratio could be explored in terms of carrier confinement, band structure, oscillator strength, spin-orbit interaction, etc.

NW homojunctions, including p-n radial/axial homojunction and controlled coherent polytypism in a single III–V NW, are elaborated following the VLS mechanism. The typical growth process of a radial or axial homojunction relies on the switching of the dopant precursors following a three-step procedure. The first dopant precursor is switched off after the growth of the first NW section following by its evacuation from the growth reactor under continuous flow of III–V organometallic precursors; then the second doping reactants starts to be injected in the chamber reactor to dope the subsequent section. When all the precursors are incorporated into the liquid catalyst, even during the dopant switching, the crystalline growth in the longitudinal direction will be favored, forming an axial homojunction (Figure 3.9(a)). An axial p-n/p-i-n homojunction provides a well-defined active region, allowing the tunable injection of electrons and holes without any light-screening phenomena (Goto et al., 2009; Lysov et al., 2011; Minot et al., 2007). On the other hand, when the second doping reactant is dissociated and absorbed at the surface of the NW, a radial homojunction is formed with an epitaxial process similar to planar growth of thin films (Figure 3.9(b)). Particular attention has been paid to radial p-i-n or p-n homostructure growths for their superior carrier collection efficiency under light illumination, where light absorption direction is orthogonal to the carrier collection (Colombo et al., 2009).

III–V NWs have potential to create an original homojunction based solely on the crystalline structure difference, i.e., ZB and WZ. This feature is totally new and specific to III–V NW synthesis, since only one crystalline structure (the cubic ZB structure) is thermodynamically stable for III–V materials. Twin-plane superlattices based on the repetition of ZB segments with constant distance between twin planes (Algra et al., 2008; Algra et al., 2011; Caroff et al., 2008) (Figure 3.8(b)) and highly reproducible polytypism with alternative WZ and ZB segments (Caroff et al., 2008; Dick, Thelander, Samuelson, & Caroff, 2010; Figure 3.8(c)) within a single III–V NW have been successfully reported, leading to advanced optical studies originated from the crystallographic inhomogeneity. In particular, twinning superlattices growth has been observed for InAs (Caroff et al., 2008), InP (Algra et al., 2008; Shen, Bando, Liu, Tang, & Golberg, 2006), and GaP (Algra et al., 2011, 2010; Xiong et al., 2006) NWs. A model based on the influence of the liquid catalyst distortion on the growth process has been proposed to explain the twinning superlattice growth mechanism as shown in Figure 3.8(a) (Algra et al., 2008; Johansson et al., 2006). NWs grow in a layer-by-layer scheme with the nucleation point located at the triple line edge. The energy for nucleus formation relies on both the liquid–solid contact angle and the tilt angle of the external facet. The polar side facets with the orientation of $\{111\}_A$ and $\{111\}_B$ are expanding or shrinking individually during the growth because they are tilted from the $\langle 111 \rangle$ vertical direction, resulting in the transition of the NW cross-section shape from hexagonal to a triangle-like shape. As a result, the side facets may change to the alternative orientation and twin planes are formed in order to relax the strain (Algra et al., 2008; Algra et al., 2011; Johansson et al., 2006; Karlsson et al., 2007), after which the triangle-like shape cross-section evolves into the hexagonal shape and the cycle starts repeating. The twinning superlattices are naturally occurring

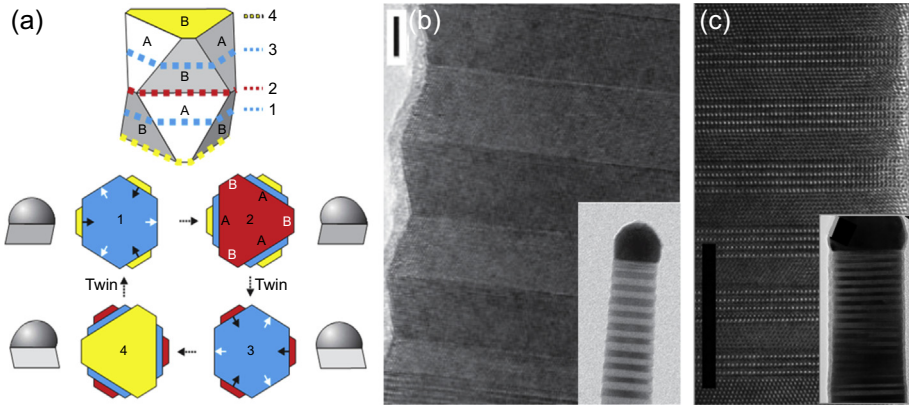


Figure 3.8 (a) Model for periodic twinning evolution in an NW showing ZB structure with nonparallel side facets. (b) TEM images of InP NW twinning superlattice with a diameter of 50 nm. Scale bar: 5 nm. (Adapted with permission from Macmillan Publishers Ltd: Nature [Algra et al. \(2008\)](#). Copyright 2008.) (c) TEM images of InAs NW superlattices with periods of alternating ZB and WZ structure (each 8 bilayers thick). Scale bar: 10 nm. (Adapted with permission from [Dick, Thelander, et al. \(2010\)](#). Copyright 2010, American Chemical Society.)

at specific growth temperatures and NW diameters (the larger the diameter, the longer the spacing between twin planes) ([Caroff et al., 2008](#)). Meanwhile, dopants, such as Zn ([Algra et al., 2008, 2011](#)), can also help to reduce the activation barrier for two-dimensional nucleation growth of ZB segment and to produce long-range ordered twinning superlattices. In this case, the spacing between twin planes is proportional to the Zn doping concentration together with the NW diameter.

NW heterojunctions also provide diversity and flexibility in the design of nanostructure and allow more complex and advanced functionalities during the bottom-up growth. A heterostructure is the combination of different materials with diverse properties. The synthesis of quasi-1D structures opens up opportunities for heterointegration compared to a thin-film counterpart. The small diameter gives NWs the inherent ability to efficiently relieve the lattice mismatch-induced strain through lateral relaxation ([Bao et al., 2008](#)). Axial and superlattice heterostructures are formed when new or alternative reactants are incorporated into the liquid alloy, resulting in longitudinal elongation, as illustrated in [Figure 3.9\(c\) and \(d\)](#). Otherwise, if the new reactants are absorbed at the NW surface, a shell will grow on the original NW surface, promoting the formation of a core-shell NW ([Figure 3.9\(e\)](#)). Changing reactants in the radial growth regime will result in the formation of a core-multi-shell geometry ([Figure 3.9\(f\)](#)). The precise control of the III-V heterostructure growth conditions enables the fabrication of custom-built NW architectures. For instance, GaAs/Al_xGa_{1-x}As radial Type I heterostructures ([Fontcuberta I Morral, Spirkoska et al., 2008](#); [Gallo et al., 2011](#); [Heigoldt et al., 2009](#); [Heiss et al., 2013](#); [Sladek et al., 2010](#); [Spirkoska, Abstreiter, & Morral, 2009](#)) are promising in the applications of high electron mobility transistors (HEMTs), photo-detector, and solar cells, where both electrons and holes tend to be localized in the lower

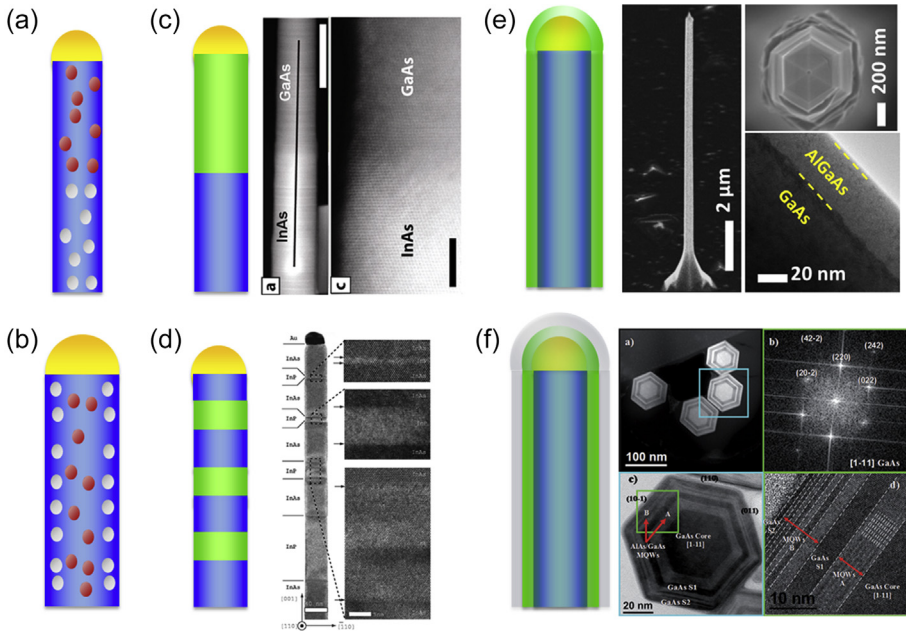


Figure 3.9 NW homojunctions and heterostructures. Axial and radial p-n homojunctions showing in (a) and (b). (c) An axial NW heterostructure with the TEM image showing an InAs-GaAs junction. (Adapted with permission from [Dick, Bolinsson, Borg, and Johansson \(2012\)](#). Copyright 2012, American Chemical Society.) (d) An NW with axial alternating materials. TEM image displaying an InAs NW containing four sequential InP barriers. (Reprinted with permission from [Björk et al. \(2002a\)](#). Copyright 2002, AIP Publishing LLC.) (e) A radial (core/shell) NW heterostructure. SEM image presenting an as-grown GaAs/AlGaAs NW and the TEM image showing a clear boundary. (f) Schematic of core-multishell NW. High angular annular dark field (HAADF) image showing cross-sections of multiple quantum well NWs, consisting of multiple alternative AlAs and GaAs shells on an GaAs core. (Adapted with permission from [Heigoldt et al. \(2009\)](#). Copyright 2009, Royal Society of Chemistry.)

bandgap material (GaAs). Alternatively, Type II staggered band alignment, e.g., GaAs/InAs ([Messing et al., 2011](#); [Ohlsson et al., 2002](#); [Panev et al., 2003](#)), formed by periodically distributed band-edge alignment, should provide better performances for photodetectors since electrons and holes could be dragged into opposite directions, hence decreasing the probability of electron–hole recombination. The uncommon broken gap type III heterostructure GaSb(p)/InAs(n) NW leads to efficient band-to-band tunneling and to possible higher current densities ([Borg et al., 2012](#)).

Recently, intersected or branched nanowires have gained paramount interests thanks to their capability of realizing interconnection during growth and offering a promising platform for low-dimensional fundamental condensed-matter physics research ([Alicea, Oreg, Refael, Oppen, & Fisher, 2011](#); [Sau, Clarke, & Tewari, 2011](#)), Self-assembly of monolithic junctions ([Dai et al., 2011](#); [Dalacu, Kam, Austing, & Poole, 2013](#); [Kang et al., 2013](#); [Plissard et al., 2013](#)) and two-step catalytically

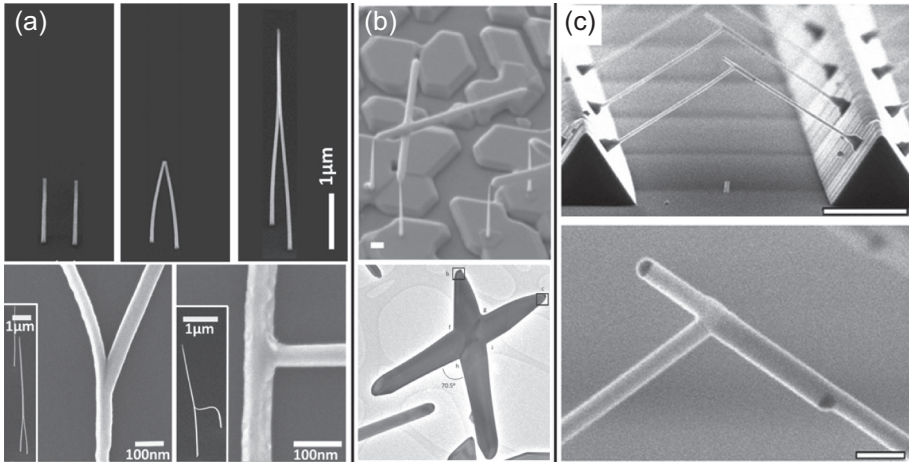


Figure 3.10 (a) Evolution of monolithic GaAs junction formation. (Reprinted with permission from Dai et al. (2011). Copyright (2011) American Chemical Society.) (b) InSb nanocrosses forming through the merging process between two InSb NWs grown on InP/InAs stems. (Adapted by permission from Macmillan Publishers Ltd: Nature Nanotechnology (Plissard et al. (2013). Copyright 2013.) (c) SEM image of a pair of connected NWs grown on InP ridges pitched at 3.5 μm. The scale bar is 1 μm. Close-up of the intersection. The scale bar is 100 nm. (Reprinted with permission from Dalacu et al. (2013). Copyright (2013) American Chemical Society.)

branched NW growth has become controllable (Dick et al., 2004; Jiang et al., 2011; Suyatin et al., 2008). Dai et al. demonstrated that self-assembly of monolithic GaAs NW junctions can be achieved by simultaneously tuning the diameter, the height, and the interdistance between two NWs to the point where the electrostatic energy between polar surfaces exceeds the mechanical energy required to bend the NWs to the point of contact (Figure 3.10(a); Dai et al., 2011).

Lately, Plissard et al. discussed the ability of horizontal InSb NWs grown from InP/InAs stems to meet and merge into T or X junctions under specific conditions (Figure 3.10(b)) and their potential for the exchange of Majorana fermions in quantum transport study (Plissard et al., 2013). Dalacu et al. reported their unique control of interconnected InAs NWs grown on InP ridge templates through selective-area growth (Figure 3.10(c)), which open up new opportunities for large-scale functional device integration (Dalacu et al., 2013).

4.2.4 Heteroepitaxial growth

The growing demand for the implementation of high-performance III–V structures into the well-established and functional silicon platform is facing technological challenges due to lattice mismatch, thermal expansion coefficient difference, and polar/nonpolar surface nature. However, the quasi 1D geometry characteristics of the NW, i.e., the large surface-to volume ratio and small diameter, promote the strain relaxation coming from lattice mismatch, thus reducing the lattice-matching

requirement existing in conventional thin-film growth, and enabling direct high-quality heteroepitaxy without introducing a buffer layer. A non-exhaustive list of lattice mismatches of III–V on non III–V is reported, e.g., GaAs (4.1%) (Bao et al., 2008; Dick, Deppert, Samuelson, Wallenberg, & Ross, 2008; Fauzia, Vincenzo, Silvia, & Faustino, 2008; Huang et al., 2010; Ihn, Ryu, & Song, 2010; Jung-Hyun et al., 2010; Kang et al., 2010; Khorenko et al., 2004; Mårtensson et al., 2004; Plissard, Larrieu, Wallart, & Caroff, 2011; Soo-Ghang, Jong-In, Young-Hun, Yong Lee, & Il-Ho, 2007; Tomioka, Motohisa, Hara, Hiruma, & Fukui, 2010), InAs (11.6%) (Chuang et al., 2007; Dayeh, Yu, & Wang, 2007c; Koblmüller et al., 2010; Mandl et al., 2006; Pratyush Das et al., 2013; Roest et al., 2006; Soo-Ghang & Jong-In, 2007; Tomioka, Motohisa, Hara, & Fukui, 2008; Wei et al., 2009), InP (8.1%) (Boles, Thompson, & Fitzgerald, 2009; Chuang et al., 2007; Dalacu et al., 2009; Mårtensson et al., 2004; Roest et al., 2006), GaP (0.37%) (Boulanger & Lapierre, 2012; Dick et al., 2008; Mårtensson et al., 2004; Roest et al., 2006), and ternary-alloy (Mattila, Hakkarainen, Lipsanen, Jiang, & Kauppinen, 2006; Mattila, Hakkarainen, Mulot, & Lipsanen, 2006; Moewe, Chuang, Crankshaw, Chase, & Chang-Hasnain, 2008; Mohseni, Maunders, Botton, & Lapierre, 2007; Ng et al., 2012; Plissard, Dick, Wallart, & Caroff, 2010; Shin et al., 2013; Svensson et al., 2008; Tomioka et al., 2010 on Si; InP on Ge (3.7%) (Bakkers et al., 2004); and even GaAs and InAs on graphite (Hong, Lee, Wu, Ruoff, & Fukui, 2012; Munshi et al., 2012). III–V NW-based devices integrated on Si, such as photodetectors (Bao et al., 2008), photovoltaics (Bao et al., 2008; Shin et al., 2013), LEDs (Svensson et al., 2008; Tomioka et al., 2010), tunneling diodes (Bessire et al., 2011), and surrounding-gate FETs (Rehnstedt, Martensson, Thelander, Samuelson, & Wernersson, 2008; Tanaka et al., 2010), have been demonstrated relying on the successful III–V/Si heteroepitaxial growth.

As discussed in Section 3.1.1, III–V NWs preferably grow on (111)B substrate in the $\langle 111 \rangle$ direction. However, due to the unpolarized surface of the Si (111) substrate, they tend to grow in the four equivalent $\langle 111 \rangle$ directions with one perpendicular to the Si substrate and three other orientations having a 19.5° angle with respect to the surface and 120° between in-plane projections of one another (Figure 3.2(a) and (b)). With the proper substrate preparation (buffer oxide etchant was used for native oxide removal) and under specific growth conditions, Wei et al. were among the first who demonstrated the growth of extremely high-density vertical Au-catalyzed GaAs and InAs NWs (Figure 3.11(a)) on Si (111) substrate, suitable for large-scale application in photovoltaics and photodetectors (Bao et al., 2008; Wei et al., 2009). To be more specific, Si^{1+} , Si^{2+} and Si^{3+} structures are usually observed on the Si (111) surface (Hattori et al., 1996; Himpfel, Mcfeely, Taleb-Ibrahimi, Yarmoff, & Hollinger, 1988). Tomioka et al. reported that InAs NWs could grow vertically on the Si (111) surface presenting only As-incorporated Si^{3+} and In-terminated Si^{1+} properties (Figure 3.11(b)), which was reconstructed under proper precursor flow and growth temperature (Tomioka et al., 2008). Recently, remarkable advances in the uniform catalyst-free growth of high-density vertical $\text{InAs}_y\text{P}_{1-y}$ NWs on an entire 2-inch Si (111) substrate have also allowed the feasibility of a heterojunction solar cell of n-type $\text{InAs}_y\text{P}_{1-y}$ and p-type Si at wafer-scale, making it compatible with industrial fabrication standards (Shin et al., 2013).

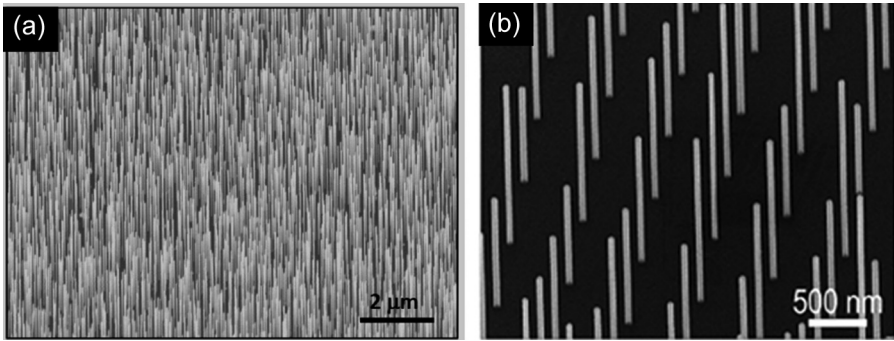


Figure 3.11 (a) 45° tilted SEM image of Au-catalyzed InAs NWs grown vertically on Si (111) substrate. (b) 45°-tilted view of InAs NW array on patterned Si substrate without catalyst. (Reprinted with permission from Tomioka et al. (2008). Copyright (2008) American Chemical Society.)

Toward the integration of high-performance III–V NW-based devices with the mature Si-based technology, it is highly desirable to be able to manage the positioning of vertical NWs during the growth. Two approaches are commonly used. The first relies on patterned arrays of metal seeds (mainly Au), serving as growth catalysts for VLS growth. However, the use of Au catalyst for III–V NWs on Si substrate was reported to have a detrimental effect on the growth, e.g., migration and oxidation of Si on Au prior to growth (Boulanger & Lapierre, 2012; Roest et al., 2006); and on some properties, e.g., Au incorporation in NW introducing deep-level traps. The second can use SA growth without introducing an exterior catalyst on a Si substrate covered by a thin SiO₂ layer with small openings. Notably, Plissard et al. reported a high-yield growth of Ga-catalyzed GaAs NW arrays on Si, demonstrating that Ga droplets formed *in situ* before the NW growth on the pre-patterned oxide-free SiO₂ openings could efficiently replace the standard Au catalyst (Plissard et al., 2011). Moreover, through Si surface engineering, III–V NWs can be selectively grown on Si even without any catalysts (Tomioka, Tanaka, Hara, Hiruma, & Fukui, 2011; Wei et al., 2009).

During the heteroepitaxial growth, misfit dislocations are usually introduced at the interface between two lattice-mismatch materials, which could be reduced by decreasing the NW diameter. Calculations explain that the strain is shared by the NW and the substrate, and mainly relaxed along the lateral direction. A critical radius exists below which coherent growth occurs without interfacial dislocation (Ertekin, Greaney, Chrzan, & Sands, 2005; Glas, 2006). A defect-free coherent growth of GaAs NW on Si with 27 nm in diameter was demonstrated in Figure 3.12(a) and (b) (Katsuhiko, Yasunori, Junichi, Shinjiroh, & Takashi, 2009). For larger-diameter NWs, Ng et al. illustrated the evolution of a defective region at the interface between InGaAs/GaAs NW and Si with increasing diameter size of 50, 120, and 740 nm. The thinner the NW, the fewer the dislocations, and shorter defective region length was observed, as shown in Figure 3.12(d–h) (Ng et al., 2012). A defective region length of 3.5 nm was observed in the NW of 50 nm in diameter at the interface

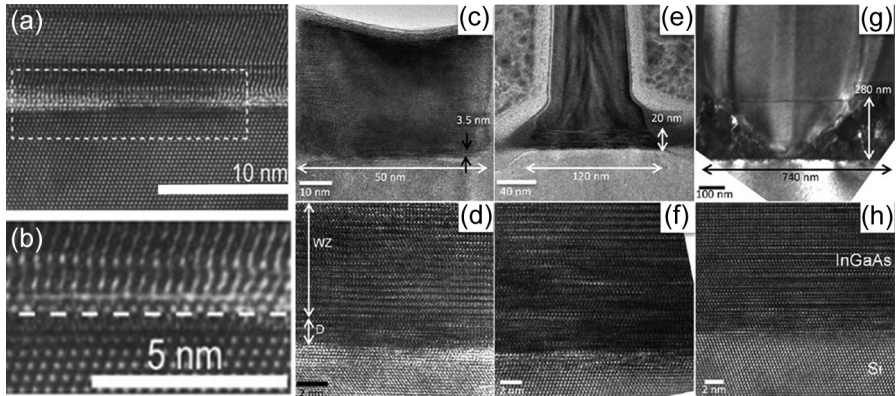


Figure 3.12 (a) Cross-sectional TEM image of a GaAs NW of 27 nm in diameter grown on Si(111). (b) The magnified image of the dashed rectangle shown in (a), showing the defect-free heterointerface of GaAs and Si(111) with 4.1% lattice mismatch. (Copyright IOP Publishing. Reproduced with permission from [Katsuhiko et al. \(2009\)](#). All rights reserved.) (c), (e), (g). TEM images of InGaAs/GaAs core–shell nanopillar with base diameters of 50, 120, and 740 nm, with the zoom-in images presented in d, f, h, respectively. The thickness of interface defective region increases from (d) 3.4 to (h) 280 nm, relaxing the 6% misfit stress between InGaAs and Si. (Reprinted with permission from [Ng et al. \(2012\)](#). Copyright (2012) American Chemical Society.)

([Figure 3.12\(d\)](#)), while a 280 nm defective region was displayed in NW with a diameter of 740 nm ([Figure 3.12\(h\)](#)).

The progress in the control of growth direction and the optimization of interface quality in the heteroepitaxial growth of III–V NWs on Si open up more opportunities in high-performance electronic and photonic applications.

3.3 Applications of III–V nanowires

Thanks to their small dimension and quasi 1D characteristics, NWs are highly considered as optoelectronic components and emerging research devices beyond CMOS by the International Technology Roadmap for Semiconductors. Among them, III–V NWs are particularly suited for the applications of FETs, photodetectors, and miniature light sources, thanks to their high electron mobility, direct bandgap, and feasibility in bandgap engineering.

3.3.1 Electronics

Silicon transistors have reduced in size by over a million times following Moore’s law since their invention in the late 1940s. Their operation speed increased by over a billion times thanks to excellent process control and recent advancements in strain engineering ([Welser, Hoyt, Takagi, & Gibbons, 1994](#)) metal gate stack and high-k dielectrics ([Wilk, Wallace, & Anthony, 2001](#)) and transistor architecture ([Hisamoto](#)

et al., 2000). However, it is expected that downscaling of the current planar Si-based technology will eventually reach its physical limits below 10 nm technology node. Among various materials and structures being investigated, III–V NW field-effect transistors (NWFETs) are considered as promising candidates on the roadmap for scaling down of electronic devices thanks to their intrinsic properties of high electron mobility and good interface quality with high-k gate dielectric. Moreover, NWs offer more degrees of freedom for the 3D integration scheme with a full control of the potential of the conducting channel. With an omega-shaped gate or gate-all-around (GAA) configuration, NWFETs offer better electrostatic control in terms of on/off current ratio, transconductance, and short channel effects compared to conventional planar transistors. Fabrication and performance of III–V NWFETs of horizontally dispersed NWs, planar as-grown NWs, and vertical NW arrays with surrounding gate will be discussed.

Intensive investigations have been carried out on lateral NWFETs where III–V NWs are successively removed from their initial grown substrate and transferred on a prepatterned SiO₂/Si substrate for future lithography process. Source and drain electrodes are then defined, followed by the global back-gate metallization (Dayeh, Aplin et al., 2007; Dayeh, Susac, Kavanagh, Yu, & Wang, 2009; Ford et al., 2010; Thelander, Caroff, Plissard, Dey, & Dick, 2011; Yang et al., 2013) or high-k material deposition and omega shape top-gate patterning (Dayeh, Aplin et al., 2007; Dey et al., 2012; Lind, Persson, Samuelson, & Wernersson, 2006; Storm, Nylund, Borgstrom et al., 2011). Progress on InAs (Dayeh, Aplin, et al., 2007; Dey et al., 2012; Ford et al., 2010; Storm, Nylund, Samuelson, & Micolich, 2011; Thelander et al., 2011), GaAs (Schricker, Davidson, Wiacek, & Korgel, 2006), InP (Storm, Nylund, Borgstrom et al., 2011), InSb (Yang et al., 2013), InAs/InP (Jiang et al., 2007), and InAs/InAsP (Lind et al., 2006) dispersed NW FETs has been thoroughly reported in the literature. Among the numerous choice of III–V materials, InAs is particularly attractive due to its high mobility at room temperature and inherent surface Fermi-level pinning in the conduction band, which allows formation of n-type ohmic contacts. Dayeh et al. performed a systematic study on InAs NWFET regarding impact of surface states (Dayeh, Soci, Yu, Yu, & Wang, 2007a, 2007b), carrier mobility (Dayeh, Aplin, et al., 2007), field-dependent transport (Dayeh, Susac, Kavanagh, Yu, & Wang, 2008), diameter dependence (Dayeh, Yu, & Wang, 2009), and influence of the crystal structure (Dayeh, Susac et al., 2009). Transfer curve hysteresis is normally observed in NW FETs due to the surface states. By reducing the gate voltage sweep rate, trapping and detrapping charge mechanism can be controlled, resulting in a reduced hysteresis. As a result, to extract the intrinsic NW transport parameters, one needs to ensure the NW surface is charge neutralized or passivated. At slow and fast sweep rate, electron mobility of $\sim 16,000 \text{ cm}^2/(\text{V}\cdot\text{s})$ and $\sim 6580 \text{ cm}^2/(\text{V}\cdot\text{s})$ are extracted, respectively, demonstrating that the slower the sweeping rate, the higher measured transconductance. Furthermore, the transconductance and the mobility are degraded at both vertical and lateral high electric field due to the enhanced phonon scattering coming from heating effects and possible morphological degradation. Lower mobility and higher average carrier concentration are observed in smaller diameter NWs caused by the presence of an electron surface accumulation layer that

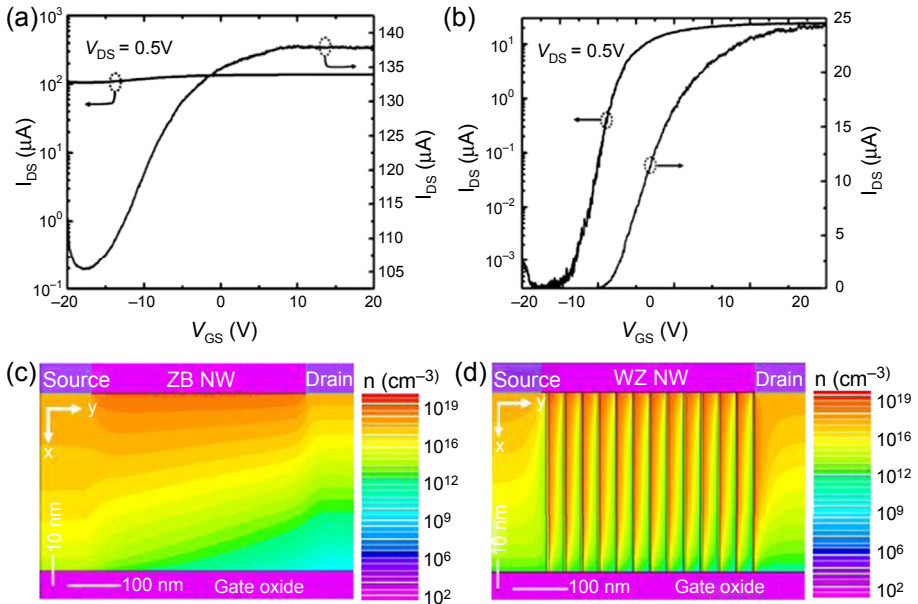


Figure 3.13 Transfer characteristics of long-channel (LSD = 3.4 μm) back-gate InAs NWFETs made from (a) pure ZB ($D_{\text{NW}} \sim 81$ nm) showing $I_{\text{on}}/I_{\text{off}} < 2$ and (b) WZ/ZB ($D_{\text{NW}} \sim 60$ nm) InAs NWs showing $I_{\text{on}}/I_{\text{off}} > 104$ at $V_{\text{DS}} = 0.5$ V. The corresponding 2D simulation in (c) and (d) showing contour plots of carrier concentration extracted at $V_{\text{DS}} = 0.5$ V and $V_{\text{GS}} = -20$ V in an InAs slab, with stronger depletion penetrating deeper across the channel body in (d). (Reprinted with permission from Dayeh, Susac et al. (2009). Copyright (2009) WILEY-VCH.)

increases the surface scattering, while higher mobility and lower average carrier concentration are expected for larger-diameter NWs due to bulk-like transport property. It is also essential to understand the correlation between the crystal phase and the electronic transport behavior, since polytypism is typically observed in III–V NWs. WZ InAs NWs with numerous SFs exhibited improvement of the on/off ratio compared to pure ZB NWs, but lower current level (Figure 3.13(a) and (b)), which was also observed by Thelander et al., where NWs with mixture of two phases presented a higher resistivity by two orders of magnitude compared to single-phase NWs (Thelander et al., 2011). The nonzero spontaneous polarization charges present at the WZ/ZB interfaces suppress carrier accumulation at the NW surface, resulting in a full depletion of the channel (Figure 3.13(d)). These results pave the way for incorporating III–V NWs into future electronic devices. With the advances in the synthesis of III–V, Li et al. achieved the self-assembly of planar $\langle 110 \rangle$ GaAs NWs on semi-insulating GaAs (100) substrate (Fortuna & Li, 2009), where GaAs NWs were capped with an AlGaAs shell (Miao & Li, 2011). Excellent transistor properties were demonstrated on such single GaAs FETs with subthreshold slopes as low as 150 mV/dec, and mobility of ~ 4100 $\text{cm}^2/(\text{V} \cdot \text{s})$.

On the other hand, vertical III–V NWFETs on III–V substrate (Bryllert, Wernersson, Froberg, & Samuelson, 2006; Thelander, Frobergfroberg, Rehnstedt, Samuelson,

& Wernersson, 2008) or on Si substrate (Rehnstedt et al., 2008; Tanaka et al., 2010; Tomioka, Yoshimura, & Fukui, 2012a, 2011) with a wrap-gate topology further improve the gate controllability and efficiently suppressed short-channel effect. An InAs vertical NWFET on InAs substrate through 3D device fabrication process was first reported in 2005 (Bryllert, Samuelson, Jensen, & Wernersson, 2005), which opened new schemes for future heteroepitaxial integration of SA-grown InAs (Bryllert et al., 2006; Rehnstedt et al., 2008; Tanaka et al., 2010; Thelander et al., 2008) (Figure 3.14(a–c)) and InGaAs (Tomioka et al., 2012a; Tomioka, Yoshimura et al., 2011) NWFET on an Si platform. Advanced optimization on the design of the NW architecture was introduced by Tomioka et al., where a complexed InGaAs/InP/InAlAs/InGaAs core-multishell structure (Tomioka et al., 2012a; Tomioka, Yoshimura et al., 2011) exhibited improved intrinsic characteristics, i.e., a higher drain current, a steep subthreshold slope (75 mV/dec), and a low drain-induced barrier lowering (35 mV/V) thanks to the shell passivation and the formation of an electron gas inside the InGaAs channel (Figure 3.14(d–f)).

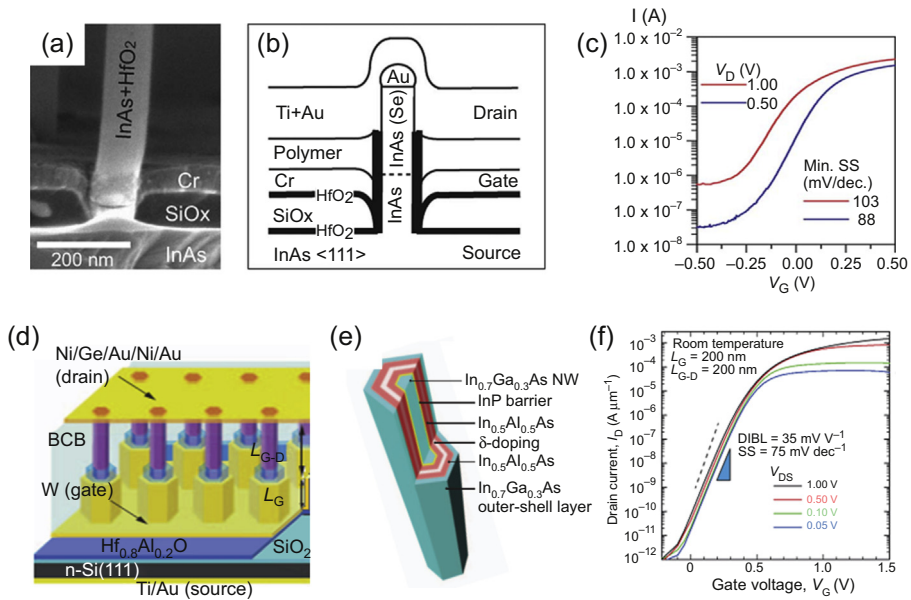


Figure 3.14 (a) Side view of a cleaved vertical InAs NWFET on InAs showing an SiO_x layer lifts the gate pad from the InAs source contact as schematized in (b), with the transfer characteristics of the device with $L_G = 50$ nm at the voltage of $V_D = 0.5$ (bottom) and 1.0 V (top) presented in (c). (Reprinted with permission from Thelander et al. (2008). Copyright 2008, IEEE.) (d) Structure of surrounding gate transistor with InGaAs/InP/InAlAs/InGaAs NWs connected in parallel with the drain metal on Si. The NW consists of InGaAs NW core wrapped with InP/InAlAs/ δ -doped InAlAs/InAlAs/InGaAs multilayers as illustrated in (e). (f) Transfer performance of this device with $L_G = 200$ nm and $L_{G-D} = 50$ nm showing low subthreshold slope (SS) and drain-induced barrier lowering (DIBL). (Adapted with permission from Macmillan Publishers Ltd: Nature (Tomioka et al. (2012a). Copyright 2012.)

3.3.2 Photonics

Among the great features of NWs, bandgap engineering of III–V alloys offers great promise for photonic applications over a wide spectral range (Hyun et al., 2013; Mi, 2009).

The 1D morphology of NWs gives them the ability to guide light, similar to optical fibers. Moreover, III–V NWs can be pushed to subwavelength diameters and exhibit better light guidance thanks to their high refractive index with respect to the surrounding environment (Hua, Motohisa, Ding, Hara, & Fukui, 2007; Maslov & Ning, 2004). The finite length of the NW intrinsically generates Fabry–Pérot resonances due to the reflection on its end-facets (Ning, 2010). However, the rather poor quality factor obtained using as-grown end-facets (Hua et al., 2007; Maslov & Ning, 2003; Yang et al., 2009) has led to resonance improvement alternatives, such as using Bragg (Chen & Towe, 2006; Zhang & Loncar, 2008) or metallic mirrors (Friedler et al., 2008, 2009). Single GaSb NW near-infrared lasers have been demonstrated for telecommunications applications (Chin et al., 2006), as has stimulated emission in InGaAs/GaAs core–shell nanopillar grown on Si (Chen et al., 2011), originated from its diameter that is larger than effective wavelength and that supports whispering gallery modes. Thanks to surface passivation offered by shell growth, lasing was observed in GaAs/GaAsP core–shell NWs at low temperature (Hua, Motohisa, Kobayashi, Hara, & Fukui, 2008), and more recently in a GaAs/AlGaAs/GaAs core–shell-cap NW at room temperature, as shown in Figure 3.15(a) and (b) (Saxena et al., 2013). However, achieving stimulated emission requires high pump power due to high losses of such lasers. Integration of the NW gain media with external cavities seems a promising route.

Possibilities offered by photonic crystals (PhCs) in terms of light confinement and guidance (Johnson, Mekis, Shanhui, & Joannopoulos, 2001) can lead to tremendous advantages when combined with bottom-up grown NWs. PhC cavities or waveguides on suspended membranes can be used as host substrate for post-positioning of the NW (Birowosuto et al., 2013; Larrue et al., 2012), or SA growing nanopillars to form PhC lasers through the bottom-up approach. For the latter, the PhC laser was fabricated by the SA growth of nanopillars made of GaAs/InGaAs/GaAs axial heterostructure with a GaInP shell on a masked GaAs substrate, as depicted in Figure 3.15(c). Room-temperature lasing action under optical pumping has been demonstrated, with a peak power of 42.5 nW (Figure 3.15(d)). By varying the pillar diameter and interpillar distance, the emission wavelength can be further tuned from 960 to 989 nm (Scofield et al., 2011).

NW is a natural candidate as gain media in LED thanks to their wide range of emission wavelengths (Duan et al., 2000; Fang, Ma, Jaw, Cohen, & Stringfellow, 1990; Hyun et al., 2013; Mattila, Hakkarainen, Mulot et al., 2006). Electrically driven LEDs have been first demonstrated using as-grown GaAs NW with p–n junctions embedded in a transparent dielectric (Haraguchi, Katsuyama, & Hiruma, 1994). A strong emitted light dependence on the polarization has been observed, in accordance with earlier experiments and theoretical predictions (Ruda & Shik, 2005; Wang et al., 2001), paving the way for polarized LEDs (Fang et al., 2011). Single NW emissions have been observed in a transferred InP wire containing an InAsP quantum dot (QD) (Minot et al., 2007; Zwiller et al., 2008) or a free-standing n-GaAs/i-InGaAs/p-AlGaAs core-multishell structure grown on Si substrate (Chuang et al., 2010).

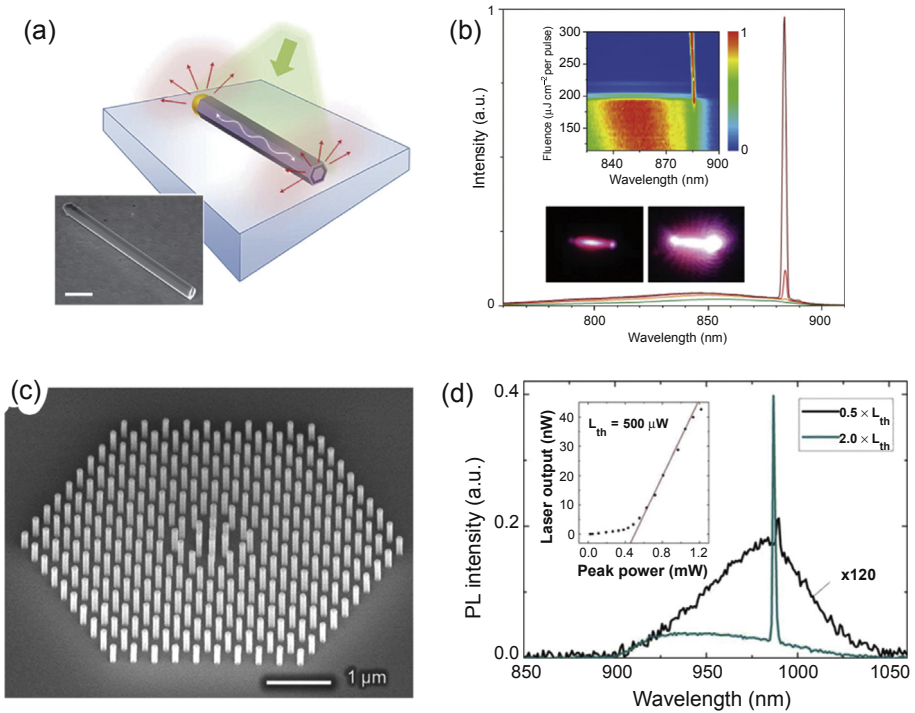


Figure 3.15 (a) Schematic and SEM image of the GaAs NW laser lying on a SiO₂/Si substrate. The NW emits in the near-infrared on the two ends under the 522 nm pulsed laser source pumping. (b) Spectra at four different optical pump powers, showing the transition from spontaneous emission at 144 and 202 μJ/cm² (lower two curves) to lasing at 240 and 288 μJ/cm² (top two). Top inset showing normalized spectral map, and bottom inset displaying optical images of the nanowire below (left) and above (right) threshold. (Adapted by permission from Macmillan Publishers Ltd: Nature Photonics (Saxena et al. (2013)). Copyright 2013.) (c) SEM image of a bottom-up grown PhC structure consisting of GaAs/InGaAs/GaAs axial hetero-structured nanopillars passivated by the InGaP shell. (d) The photoluminescence emission of this structure is presented below threshold (curve magnified by 120) and above threshold (exhibiting a sharp peak). Inset shows the output power dependence on the pump power. (Reprinted with permission from Scofield et al. (2011)). Copyright (2011) American Chemical Society.)

In addition, a core-multishell GaAs/AlGaAs NW array on Si has been used in LEDs, exhibiting an electroluminescence (EL) threshold current of 0.4 A/cm² at 1.9 V and superluminescence exhibited as the superlinear increment of EL intensity with current injection (Tomioka et al., 2010). Similarly, EL has also been observed in GaAs/InGaP radial heterostructure NW array grown on Si, although the higher intensity of EL emission was reported in the NW array epitaxially grown on GaP substrate (Svensson et al., 2008). To note that no EL from GaP NW has been shown yet, a recent report about direct bandgap WZ GaP NW growth promises further broadening of emission range to the green wavelengths (Assali et al., 2013).

Table 3.2 First orbital Bohr radius of the different non-nitride III–V semiconductor materials

	InP	InAs	InSb	GaP	GaAs	GaSb
a_B (Å)	120	494	1017	50	155	306

Values extracted from [Adachi \(2004\)](#).

The insertion of QD regions and the morphology control during the NW growth makes it possible to tune the spontaneous emission rate in NWs, and thus opens up application in quantum information processing by acting as single-photon sources for the generation of qubits ([Bleuse et al., 2011](#); [Friedler et al., 2009](#)). In earlier studies, bright emission of QDs has been reported in GaP NWs with GaAsP segments ([Borgström, Zwiller, Müller, & Imamoglu, 2005](#)) and in a GaAs NW with InAs QD insertion ([Panev et al., 2003](#)). Single-photon sources using NWs have been reported in several different systems such as AlGaAs NWs with a GaAs QD ([Heinrich et al., 2010](#)), InGaAs QD ([Makhonin et al., 2013](#)), a GaAs NW with an InAs QD ([Claudon et al., 2010](#)), and an InP NW with an InAsP QD ([Reimer et al., 2012](#)).

Thanks to the growth versatility, the diameter of the wires can be tuned to access the quantum regime. The exciton radius (or Bohr radius) expresses the limit at which quantum effects take place in the system, such as radial quantum confinement. This limit can be calculated using the reduced mass and electron mass for each material ([Adachi, 2004](#)). [Table 3.2](#) gives a summary of Bohr radius for the main III–V materials.

The quantum confinement effect has been experimentally studied in single-phase material NWs ([Gudiksen, Wang, & Lieber, 2002](#); [Zhang, Tateno et al., 2009](#)), polytypic NWs ([Pemasiri et al., 2009](#)), and axial heterostructures ([Haraguchi et al., 1994](#)). The measured photoluminescence results are in agreement with those predicted by theoretical investigations: a shift towards lower energy with increasing diameter, along with a strong anisotropic polarization of light absorbed or emitted by NWs ([Ruda & Shik, 2005](#); [Wu, Neaton, & Grossman, 2008](#)). More recently, attention has been paid to the study of nonlinear processes in NWs, such as two-photon absorption-related photoluminescence, or second and third harmonic generation ([Chen et al., 2010](#); [Grange et al., 2012](#); [Wang et al., 2011](#)). A thorough theoretical study of the influence of the wire geometry has shown a strong anisotropy, which differs from one nonlinear process to the other ([Cisek, Barzda, Ruda, & Shik, 2011](#); [Ruda & Shik, 2007](#)). Nonlinearities have been found in wire-like quantum dashes to create a two-photon induced laser ([Capua, Karni, Eisenstein, Reithmaier, & Yvind, 2012](#)), promising potential applications based on nonlinear optical phenomena.

3.3.3 Opto-electronics

With bandgap engineering and controllable doping during bottom-up growth, along with their large surface-to-volume ratio, NWs promise an enhanced sensitivity to light

and become excellent candidates for optoelectronic applications, such as photodetector and photovoltaics (Borgstro et al., 2011; Garnett, Brongersma, Cui, & McGehee, 2011; Hannah et al., 2013; Hyun et al., 2013; Joyce et al., 2011; Soci et al., 2010).

III–V NW direct-bandgap photodetectors gain optical absorption from ultraviolet to infrared. Large-bandgap material (III–N) enables the functionalities in the ultraviolet and visible spectral region, which will not be described here. In 2001, Lieber et al. first reported measurement of integrated photocurrent in a single InP NW (Duan et al., 2001). Following that, an InP photoconductor was demonstrated in nanoneedles grown on a nonsingle crystalline Si platform (Kobayashi et al., 2007), photocurrent spectroscopy was used to study the crystalline structure of a single InP NW at room temperature (Maharjan et al., 2009), and more advanced single-photon detection relying on avalanche amplification of single excitons has been achieved in an InP NW (Bulgarini et al., 2012). The photoconductive response of GaAs systems is also widely investigated, include single GaAs NWs (Kim et al., 2011; Thunich et al., 2009; Wang, 2013), GaAs p-i-n radial structures (Colombo et al., 2009), GaAs/AlGaAs core–shell NWs (Chen et al., 2013; Chuang et al., 2010; Gallo et al., 2011; Jiang et al., 2013; Kim, Dheeraj, Fimland, & Weman, 2013; Persano et al., 2011), and GaAs/InGaP/GaAs core-multishell NWs (Gutsche et al., 2012). Apart from those aforementioned near-infrared light detections (photon energy of 0.9–1.7 eV), narrow bandgap materials (such as InAs) extend the application to the mid-infrared spectral region (photon energy of 0.15–0.4 eV). Though progress of InAs optoelectronic and photonic applications are limited by strong Auger recombination and a nonradiative surface, an InAsP shell could effectively reduce surface recombination and confine the carriers (Pettersson et al., 2006; Treu et al., 2013).

Another promising application lies in solar cells. Planar III–V compound (GaAs) structures can dramatically reduce the material thickness required to absorb 90% of power (optical thickness) to submicron region compared with Si (Kayes, Atwater, & Lewis, 2005). Moreover, NW geometry benefits light harvesting thanks to its long lengths in the direction of incident light, promoting absorption; and small lengths in the radial directions, facilitating carrier collection. Utilizing different III–V materials and heterostructures, a wide range of absorption wavelengths can also be accessible (Goto et al., 2009; Ren et al., 2010; Wei et al., 2009). Single NW solar cells have been experimentally realized in GaAs p-i-n NWs (Colombo et al., 2009; Krogstrup et al., 2013), GaAsP p-i-n NWs (Holm et al., 2013), GaAs/InGaP/GaAs core-multishell NWs (Gutsche et al., 2012), and Schottky contacted GaAs NWs (Han et al., 2012).

Theoretical calculations predict that structures of solar cells affect the light conversion efficiency: dispersed GaAs NWs on host substrate present lower quantum efficiency because of reduced coupling of incident light in the NW (Heiss & Fontcuberta i Morral, 2011), while as-grown GaAs NW solar cells exhibits a theoretical limiting efficiency of 30% (Lapierre, 2011a). Similar trends have been observed in the experimental results. Figure 3.16(a) shows a single p-i-n GaAsP core–shell NW solar cell lying on an SiO₂/Si substrate (Holm et al., 2013). The characterization of this device (Figure 3.16(b)) presents an overall efficiency as high as 10.2%. However, this value is still lower than the theoretically predicted Shockley–Queisser limit of for a semiconductor bandgap of 1.7 eV (Shockley & Queisser, 1961), which

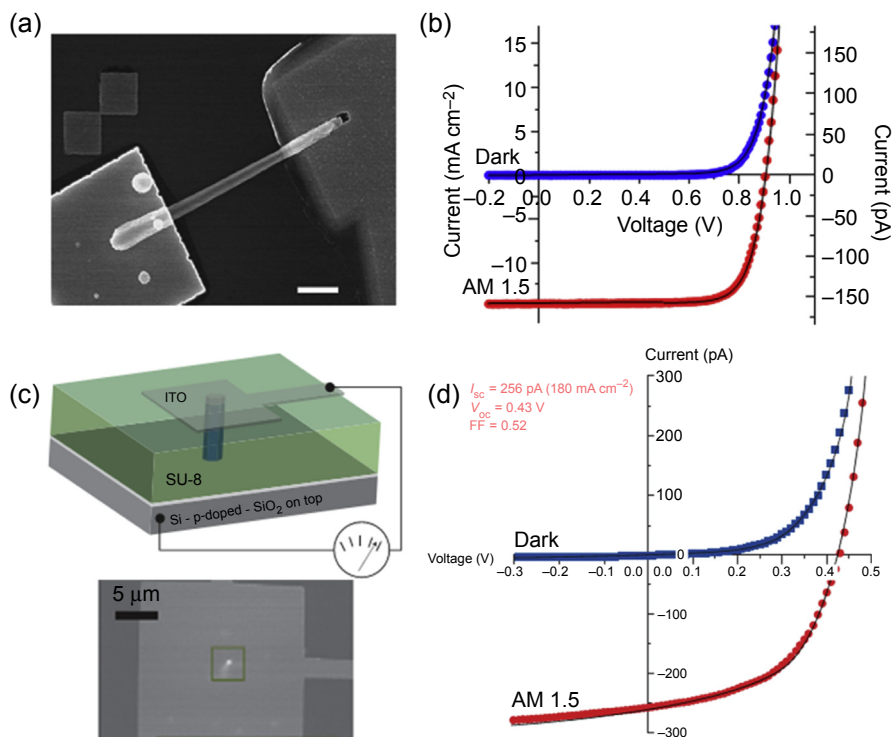


Figure 3.16 Single NW solar cell. (a) SEM image of the device with GaAsP p-i-n core-shell NW connected to metallic pads. Scale bar is 1 μm . (b) I–V characteristics of the device under dark (top curve) and AM1.5G illumination (bottom curve). Data fit is represented in full lines. (Adapted by permission from Macmillan Publishers Ltd: Nature Communications [Holm et al. \(2013\)](#). Copyright 2013.) (c) Schematic of a vertical single NW solar cell consists of a GaAs radial p-i-n NW epitaxially grown on a p-type Si substrate; SEM top view of the device. (d) I–V performance of the device in the dark and under AM 1.5G illumination. (Adapted by permission from Macmillan Publishers Ltd: Nature Photonics [Krogstrup et al. \(2013\)](#). Copyright 2013.)

resulted from the dispersed device configuration. In comparison, a solar cell based on a p-i-n GaAs core-shell NW on p-Si substrate boosts the solar conversion efficiency to 40%, as illustrated in [Figure 3.16\(c\) and \(d\)](#) ([Krogstrup et al., 2013](#)). This remarkable efficiency exceeds the GaAs Shockley-Queisser limit of 33.5% ([Miller, Yablonovitch, & Kurtz, 2012](#)), due to the vertical configuration and enhanced resonant absorption effect.

More recently, devices integrating III–V NW structures heteroepitaxially grown on Si substrates have attracted attention; these are compatible with standard Si technology, and may possibly improve cell efficiency and lower the cost at the same time ([Bu et al., 2013](#); [Foster & Wilson, 2013](#); [Lapierre, 2011b](#)). In combination with NW arrays, the reflectance can be dramatically reduced. Due to strong scattering of the incident light inside the array, more photons are absorbed before being scattered out; this results in

the improved light-trapping properties and absorbance of solar-cell devices (Anttu & Xu, 2013; Muskens et al., 2009; Muskens, Rivas, Algra, Bakkers, & Lagendijk, 2008; Wu, Anttu, Xu, Samuelson, & Pistol, 2012). Meanwhile, NW arrays can also be designed for a certain efficiency and absorption spectral range, since large-diameter NWs absorb light in a longer wavelength region than small diameter, and dense NW arrays reflect less light than sparse arrays (Wu et al., 2012). An array of GaAs NWs grown on an Si substrate has been reported with 8.1% efficiency (Hu et al., 2013), along with an InAs NW array grown on Si that exhibited a 2.5% efficiency (Wei et al., 2009). GaAsP core-shell n-p junction grown on a (001)-oriented Si substrate have also shown photovoltaic properties (Tchernycheva et al., 2012).

A better understanding of performance limitations in terms of inherent physical properties and NW growth and device structure design, will certainly lead to a wide use of III-V NW devices.

3.3.4 Quantum transport

NWs enable the formation of abrupt, defect-free interfaces between lattice-mismatch semiconductors, which opens up new opportunities for the fundamental investigations of low-dimensional quantum devices based on III-V heterostructures.

Tunnel diodes are key components in multijunction solar cells, low-power memory devices, and low-power tunnel FETs (TFETs). III-V NW tunnel diodes based on staggered (InAs/Si (Bessire et al., 2011; Björk et al., 2010), InP/GaAs (Wallentin et al., 2010), InAs/InP (Björk, Ohlsson, Thelander, et al., 2002)) and broken (GaSb/InAs (Borg et al., 2012)) type-II band alignment were investigated in details in terms of tunnel process and impact of traps from defects and dislocations at the junction interface.

In conventional FETs, carrier transport is limited by thermionic injection. SS is defined as:

$$SS = \left[\frac{d(\log_{10} I_D)}{dV_G} \right]^{-1} \quad (3.3)$$

where $\ln 10 \cdot \frac{kT}{q} \cong 60\text{mV}$. As a result, the minimum SS will be 60 mV/dec, indicating that traditional FETs require at least 60 mV of gate voltage to increase the current density by one order of magnitude. In comparison, carrier transport in TFETs follows band-to-band-tunneling (BTBT) through the space charge region of the junction, resulting possibly in an SS lower than 60 mV/dec. Note that SS is constant over a smaller applied gate-source bias (Ionescu & Riel, 2011) when compared to conventional FETs. As a result, lower supply voltage and power consumption are required. However, TFETs usually suffer from low On current, which can be overcome by using III-V NWs, since their low effective-mass and band engineering are expected to increase the transmission probability, and then On current (Ionescu & Riel, 2011). Superior electrical transport performance has been successfully demonstrated in TFETs based on InAs NWs on Si (lowest SS = 21 mV/dec) (Ionescu & Riel, 2011; Riel et al., 2012; Tomioka & Fukui, 2011; Tomioka,

Table 3.3 Direct bandgap energy for the two crystalline phases, common dopant element and main applications of the different undoped non-nitride III–V nanowire materials

Material	Direct bandgap energy (eV)		Main applications
	ZB	WZ	
InP	@0 K 1.42 Vurgaftman, Meyer, and Ram-Mohan (2001), Mishra et al. (2007), and Ikejiri, Kitauchi, Tomioka, Motohisa, and Fukui (2011) @300 K (1.34–1.35) Adachi (1989) and Madelung (2004)	@0 K (1.47–1.50) De and Pryor (2010), Mishra et al. (2007), and Ikejiri et al. (2011) @300 K 1.43 Mishra et al. (2007)	Laser: InP/InAs/InP axial heterostructure Birowosuto et al. (2013). LED: InP with InAsP quantum dot Minot et al. (2007). Single-photon source: InAsP QD in InP NW Reimer et al. (2012). Quantum effect: InP Gudiksen, Wang et al. (2002), polytypic InP Pemasiri et al. (2009). Nonlinear processes: InP Wang et al. (2011). Photodetector: InP Kobayashi et al. (2007). Single-photon detector: InP Bulgarini et al. (2012). NWFET: InP Storm, Nylund, Borgstrom et al. (2011). Tunnel diode: InP/GaAs axial heterostructure Wallentin et al. (2010). TFET: n-InP/p-GaAs axial heterostructure Ganjipour, Wallentin et al. (2012).
InAs	@0 K 0.42 Fang et al. (1990) and Vurgaftman et al. (2001) @300 K (0.35–0.36) Adachi (1989), Vurgaftman et al. (2001)	@0 K (0.47–0.48) De and Pryor (2010), Zanolli, Fuchs, Furthmüller, Von Barth, and Bechstedt (2007)	Photodetector: InAs/InAsP axial heterostructure Pettersson et al. (2006). Solar cell: InAs Wei et al. (2009). NWFET: InAs Dayeh, Aplin et al. (2007), Thelander et al. (2011), Ford et al. (2010), Dey et al. (2012), and Storm, Nylund, Samuelson et al., 2011, InAs/InP core–shell Jiang et al. (2007), InAs/InAsP/InAs axial heterostructure Lind et al. (2006), vertical InAs Tanaka et al. (2010), Rehnstedt et al. (2008), Bryllert et al. (2006), and Thelander et al. (2008). Tunnel diode: InAs NW on Si Bessire et al. (2011) and Björk et al. (2010), InAs QD bounded with InP barrier in InAs NW Björk, Ohlsson, Thelander et al. (2002). TFET: InAs NW on Si Tomioka et al. (2012b), Tomioka and Fukui

Continued

Table 3.3 Continued

Material	Direct bandgap energy (eV)		Main applications
	ZB	WZ	
InSb	@0 K 0.24 Littler and Seiler (1985) and Adachi (2004) @300 K (0.17–0.18) Adachi (1989) , Littler and Seiler (1985) , Vurgaftman et al. (2001) , and Madelung (2004)	@0 K 0.287 De and Pryor (2010)	(2011), Riel et al. (2012) , and Ionescu and Riel (2011) . SET: InAs QD bounded with InP barrier in InAs NW Thelander et al. (2003) . IR detector: InSb Dey, Svensson et al. (2013) . NWFET: p-InSb Yang et al. (2013) . Superconductor: InSb Tomioka, Yoshimura, and Fukui (2013) , InSb nanocrosses Plissard et al. (2013) .
GaP	@0 K 2.866 Zollner et al. (1993) @300 K 2.76(mean value) Zollner et al. (1993)^a	@0 K (2.09–2.11) Assali et al. (2013)	Single-photon source: GaAsP segments in GaP wire Borgström et al. (2005) .
GaAs	@0 K 1.52 Vurgaftman et al. (2001) , Blakemore (1982) , Madelung (2004) , and Adachi (2004) @300 K (1.42–1.44)	@0 K (1.50–1.55) De and Pryor (2010) , Ketterer et al. (2011) , and Murayama and Nakayama (1994) @300 K 1.39 Ketterer et al. (2011)	Laser: InGaAs/GaAs core–shell Chen et al. (2011) , GaAs/GaAsP core-shell Hua et al. (2008) , GaAs/InGaAs/GaAs axial heterostructure with GaInP shell Scofield et al. (2011) . LED: p-n junction GaAs nanowire Haraguchi et al. (1994) , GaAs/InGaP radial heterostructure Svensson et al. (2008) , GaAs/AlGaAs core-multishell Tomioka et al. (2010) . Single-photon source: InAs quantum dot in GaAs nanowire Claudon et al. (2010) and Panev et al. (2003) , AlGaAs with GaAs QD

GaSb	<p>Blakemore (1982) and Adachi (1989)</p> <p>@0 K (0.81–0.82) Vurgaftman et al. (2001), Madelung (2004), and Adachi (2004)</p> <p>@300 K (0.72–0.75) Adachi (1989) and Vurgaftman et al. (2001), Madelung (2004), and Adachi (2004)</p>	<p>@0 K 0.509 De and Pryor (2010)</p>	<p>Heinrich et al. (2010), InGaAs QD in GaAs NW Makhonin et al. (2013), Quantum effects: GaAs Zhang, Tateno et al. (2009), P-n junction GaAs Haraguchi et al. (1994). Nonlinear processes: GaAs Grange et al. (2012) and Chen et al. (2010). Photodetector: GaAs/InGaP/GaAs core-multishell Gutsche et al. (2012), GaAs/AlGaAs core–shell Gallo et al. (2011), GaAs Wang (2013), avalanche in GaAs-based heterostructure Chuang et al. (2010). Solar cell: P-i-n GaAs Krogstrup et al. (2013) and Colombo et al. (2009), p-n radial GaAs (Czaban, Thompson, and Lapierre (2008), GaAs/GaInP/GaAs core-multishell Gutsche et al. (2012), GaAs Han et al. (2012) and Hu et al. (2013), GaAs/GaInP core-multishell Nakai, Yoshimura, Tomioka, and Fukui (2013), p-i-n GaAsP core–shell Holm et al. (2013), GaAsP core–shell Tchemycheva et al. (2012). NWFET: GaAs Schricker et al. (2006) and Fortuna and Li (2009). Tunnel diode: GaSb/InAs(Sb) axial heterostructure Borg et al. (2012). TFET: GaSb/InAs(Sb) axial heterostructure Dey, Borg et al. (2013). SHT: p-type GaSb Ganjipour et al. (2011).</p>
------	---	---------------------------------------	---

^aIndirect energy–gap for intrinsic material.

Yoshimura, & Fukui, 2012b), InP/GaAs heterostructure NWs (highest $I_{\text{on}}/I_{\text{off}} = 10^7$) (Ganjipour, Wallentin, Borgström, Samuelson, & Thelander, 2012), and GaSb/InAs NWs (maximum drive current of $310 \mu\text{A}/\mu\text{m}$ for $V_{\text{DS}} = 0.5 \text{ V}$ at RT, lowest SS of $17 \text{ mV}/\text{dec}$ at 4.2 K) (Dey, Borg, et al., 2013).

At the same time, intense efforts have been carried out on single-electron transistors (SETs), where one electron at a time tunnels through a small island connected to two leads via tunnel junctions. It can be used for sensitive charge detectors, spintronics, and quantum computation. An InAs(QDs)/InP(barrier) NW-based SET exhibited a Coulomb blockade single-island transistor signature at liquid helium temperature (4.2 K), which was not observed in homogeneous InAs NWs (Thelander et al., 2003). In the case of a single-hole transistor (SHT), Ganjipour et al. demonstrated a p-type GaSb NW with close source/drain contacts that showed an infinite resistance for V_{DS} between -5 mV and 5 mV , while a series of Coulomb peaks were detected as a function of back-gate voltage at $V_{\text{DS}} = 0.1 \text{ mV}$.

3.4 Conclusion

III–V nanowire bottom-up growth mechanisms and methods are summarized. A comprehensive understanding of their crystallographic properties (i.e., defects, doping, homo- and heterojunctions, and heteroepitaxial growth) paves the way for diverse applications in electronics, photonics, optoelectronics, and quantum transport. The fundamental studies and superior performance demonstrated in single-nanowire devices opens up possibilities in large-scale nanowire device integration when combined with selective-area growth, aiming at transferring technology from the laboratory to practical implementations.

References

- Adachi, S. (1989). Optical dispersion relations for GaP, GaAs, GaSb, InP, InAs, InSb, $\text{Al}_x\text{Ga}_{1-x}\text{As}$, and $\text{In}_{1-x}\text{Ga}_x\text{As}_y\text{P}_{1-y}$. *Journal of Applied Physics*, *66*, 6030–6040.
- Adachi, S. (2004). *Handbook on physical properties of semiconductors*. Kluwer Academic Publishers.
- Akiyama, T., Sano, K., Nakamura, K., & Ito, T. (2006). An empirical potential approach to wurtzite-zinc-blende polytypism in group III-V semiconductor nanowires. *Japanese Journal of Applied Physics Part 2-Letters & Express Letters*, *45*, L275–L278.
- Algra, R. E., Verheijen, M. A., Borgström, M. T., Feiner, L.-F., Immink, G., Van Enckevort, W. J. P., et al. (2008). Twinning superlattices in indium phosphide nanowires. *Nature*, *456*, 369–372.
- Algra, R. E., Verheijen, M. A., Feiner, L.-F., Immink, G. G. W., Enckevort, W. J. P. V., Vlieg, E., et al. (2011). The role of surface energies and chemical potential during nanowire growth. *Nano Letters*, *11*, 1259–1264.
- Algra, R. E., Verheijen, M. A., Feiner, L.-F., Immink, G. G. W., Theissmann, R., Enckevort, W. J. P. V., et al. (2010). Paired twins and $\{112\}$ morphology in GaP nanowires. *Nano Letters*, *10*, 2349–2356.

- Alicea, J., Oreg, Y., Refael, G., Oppen, F. V., & Fisher, M. P. A. (2011). Non-Abelian statistics and topological quantum information processing in 1D wire networks. *Nature Physics*, *7*, 412–417.
- Anttu, N., & Xu, H. Q. (2013). Efficient light management in vertical nanowire arrays for photovoltaics. *Optics Express*, *21*, A558–A575.
- Assali, S., Zardo, I., Plissard, S., Kriegner, D., Verheijen, M. A., Bauer, G., et al. (2013). Direct band gap wurtzite gallium phosphide nanowires. *Nano Letters*, *13*, 1559–1563.
- Astromskas, G., Storm, K., Karlström, O., Caroff, P., Borgström, M., & Wernersson, L.-E. (2010). Doping incorporation in InAs nanowires characterized by capacitance measurements. *Journal of Applied Physics*, *108*, 054306.
- Bakkers, E. P. A. M., Van Dam, J. A., De Franceschi, S., Kouwenhoven, L. P., Kaiser, M., Verheijen, M., et al. (2004). Epitaxial growth of InP nanowires on germanium. *Nature Materials*, *3*, 769–773.
- Bao, X. Y., Soci, C., Susac, D., Bratvold, J., Aplin, D. P., Wei, W., et al. (2008). Heteroepitaxial growth of vertical GaAs nanowires on Si(111) substrates by metal-organic chemical vapor deposition. *Nano Letters*, *8*, 3755–3760.
- Bessire, C. D., Björk, M. T., Schmid, H., Schenk, A., Reuter, K. B., & Riel, H. (2011). Trap-assisted tunneling in Si-InAs nanowire heterojunction tunnel diodes. *Nano Letters*, *11*, 4195–4199.
- Bhunia, S., Kawamura, T., Fujikawa, S., Tokushima, K., & Watanabe, Y. (2004). Free-standing and vertically aligned InP nanowires grown by metalorganic vapor phase epitaxy. *Physica E: Low-dimensional Systems and Nanostructures*, *21*, 583–587.
- Birowosuto, M. D., Yokoo, A., Zhang, G., Kuramochi, E., Taniyama, H., Takiguchi, M., et al. (2013). Position controlled nanocavity using a single nanowire in photonic crystals. In *Lasers and electro-optics Pacific Rim (CLEO-PR), 2013 conference on, June 30 2013–July 4 2013* (pp. 1–2).
- Björk, M. T., Ohlsson, B. J., Sass, T., Persson, A. I., Thelander, C., Magnusson, M. H., et al. (2002a). One-dimensional heterostructures in semiconductor nanowhiskers. *Applied Physics Letters*, *80*, 1058–1060.
- Björk, M. T., Ohlsson, B. J., Sass, T., Persson, A. I., Thelander, C., Magnusson, M. H., et al. (2002b). One-dimensional steeplechase for electrons realized. *Nano Letters*, *2*, 87–89.
- Björk, M. T., Ohlsson, B. J., Thelander, C., Persson, A. I., Deppert, K., Wallenberg, L. R., et al. (2002). Nanowire resonant tunneling diodes. *Applied Physics Letters*, *81*, 4458–4460.
- Björk, M. T., Schmid, H., Bessire, C. D., Moselund, K. E., Ghoneim, H., Karg, S., et al. (2010). Si–InAs heterojunction Esaki tunnel diodes with high current densities. *Applied Physics Letters*, *97*, 163501.
- Blakemore, J. S. (1982). Semiconducting and other major properties of gallium arsenide. *Journal of Applied Physics*, *53*, R123–R181.
- Blouse, J., Claudon, J., Creasey, M., Malik, N. S., Gérard, J.-M., Maksymov, I., et al. (2011). Inhibition, enhancement, and control of spontaneous emission in photonic nanowires. *Physical Review Letters*, *106*, 103601.
- Boles, S. T., Thompson, C. V., & Fitzgerald, E. A. (2009). Influence of indium and phosphine on Au-catalyzed InP nanowire growth on Si substrates. *Journal of Crystal Growth*, *311*, 1446–1450.
- Bolinsson, J., Ouattara, L., Hofer, W. A., Skold, N., Lundgren, E., Gustafsson, A., et al. (2009). Direct observation of atomic scale surface relaxation in ortho twin structures in GaAs by XSTM. *Journal of Physics: Condensed Matter: An Institute of Physics Journal*, *21*, 055404.

- Borg, B. M., Ek, M., Ganjipour, B., Dey, A. W., Dick, K. A., Wernersson, L.-E., et al. (2012). Influence of doping on the electronic transport in GaSb/InAs(Sb) nanowire tunnel devices. *Applied Physics Letters*, *101*, 043508.
- Borgstrom, M. T., Immink, G., Ketelaars, B., Algra, R., & Bakkerserik, P. A. M. (2007). Synergetic nanowire growth. *Nature Nanotechnology*, *2*, 541–544.
- Borgström, M. T., Verheijen, M. A., Immink, G., Smet, T. D., & Bakkers, E. P. A. M. (2006). Interface study on heterostructured GaP–GaAs nanowires. *Nanotechnology*, *17*, 4010.
- Borgström, M. T., Zwiller, V., Müller, E., & Imamoglu, A. (2005). Optically bright quantum dots in single nanowires. *Nano Letters*, *5*, 1439–1443.
- Borgstrom, M. T., Wallentin, J., Heurlin, M., Fa, X., Lt, S., Wickert, P., et al. (2011). Nanowires with promise for photovoltaics. *IEEE Journal of Selected Topics in Quantum Electronics*, *17*, 1050–1061.
- Borschel, C., Messing, M. E., Borgström, M. T., Paschoal, W., Wallentin, J., Kumar, S., et al. (2011). A new route toward semiconductor nanospintronics: highly Mn-Doped GaAs nanowires realized by ion-implantation under dynamic annealing conditions. *Nano Letters*, *11*, 3935–3940.
- Boulanger, J. P., & Lapierre, R. R. (2012). Patterned gold-assisted growth of GaP nanowires on Si. *Semiconductor Science and Technology*, *27*, 035002.
- Bryllert, T., Samuelson, L., Jensen, L. E., & Wernersson, L. E. (2005). Vertical high mobility wrap-gated InAs nanowire transistor. In *Device research conference digest, 2005. DRC '05. 63rd, 22–22 June 2005'* (pp. 157–158).
- Bryllert, T., Wernersson, L. E., Froberg, L. E., & Samuelson, L. (2006). Vertical high-mobility wrap-gated InAs nanowire transistor. *IEEE Electron Device Letters*, *27*, 323–325.
- Bulgarini, G., Reimer, M. E., Hocevar, M., Bakkers, E. P. A. M., Kouwenhoven, L. P., & Zwiller, V. (2012). Avalanche amplification of a single exciton in a semiconductor nanowire. *Nature Photonics*, *6*, 455–458.
- Bu, S., Li, X., Wen, L., Zeng, X., Zhao, Y., Wang, W., et al. (2013). Optical and electrical simulations of two-junction III-V nanowires on Si solar cell. *Applied Physics Letters*, *102*, 031106.
- Capua, A., Karni, O., Eisenstein, G., Reithmaier, J. P., & Yvind, K. (2012). Extreme nonlinearities in InAs/InP nanowire gain media: the two-photon induced laser. *Optics Express*, *20*, 5987–5992.
- Caroff, P., Bolinsson, J., & Johansson, J. (2011). Crystal phases in III-V nanowires: from random toward engineered polytypism. *IEEE Journal of Selected Topics in Quantum Electronics*, *17*, 829–846.
- Caroff, P., Dick, K. A., Johansson, J., Messing, M. E., Deppert, K., & Samuelson, L. (2008). Controlled polytypic and twin-plane superlattices in III-V nanowires. *Nature Nanotechnology*, *4*, 50–55.
- Casadei, A., Krogstrup, P., Heiss, M., Röhr, J. A., Colombo, C., Ruelle, T., et al. (2013). Doping incorporation paths in catalyst-free Be-doped GaAs nanowires. *Applied Physics Letters*, *102*, 013117.
- Chen, R., Crankshaw, S., Tran, T., Chuang, L. C., Moewe, M., & Chang-Hasnain, C. (2010). Second-harmonic generation from a single wurtzite GaAs nanoneedle. *Applied Physics Letters*, *96*, 051110.
- Chen, G., Sun, G., Ding, Y. J., Prete, P., Miccoli, I., Lovergine, N., et al. (2013). Direct measurement of band edge discontinuity in individual core-shell nanowires by photocurrent spectroscopy. *Nano letters*, *13*, 4152–4157.
- Chen, L., & Towe, E. (2006). Nanowire lasers with distributed-Bragg-reflector mirrors. *Applied Physics Letters*, *89*, 053125.

- Chen, R., Tran, T.-T. D., Ng, K., Ko, W. S., Chuang, L. C., Sedgwick, F. G., et al. (2011). Nanolasers grown on silicon. *Nature Photonics*, *5*, 170–175.
- Chin, A. H., Vaddiraju, S., Maslov, A. V., Ning, C. Z., Sunkara, M. K., & Meyyappan, M. (2006). Near-infrared semiconductor subwavelength-wire lasers. *Applied Physics Letters*, *88*, 163115.
- Chuang, L. C., Moewe, M., Chase, C., Kobayashi, N. P., Chang-Hasnain, C., & Crankshaw, S. (2007). Critical diameter for III-V nanowires grown on lattice-mismatched substrates. *Applied Physics Letters*, *90*, 043115.
- Chuang, L. C., Sedgwick, F. G., Chen, R., Ko, W. S., Moewe, M., Ng, K. W., et al. (2010). GaAs-based nanoneedle light emitting diode and avalanche photodiode monolithically integrated on a silicon substrate. *Nano Letters*, *11*, 385–390.
- Cirlin, G., Bouravleuv, A., Soshnikov, I., Samsonenko, Y. B., Dubrovskii, V., Arakcheeva, E., et al. (2009). Photovoltaic properties of p-Doped GaAs nanowire arrays grown on n-type GaAs(111)B substrate. *Nanoscale Research Letters*, *5*, 360–363.
- Cisek, R., Barzda, V., Ruda, H. E., & Shik, A. (2011). Nonlinear optical properties of semiconductor nanowires. *IEEE Journal of Selected Topics in Quantum Electronics*, *17*, 915–921.
- Claudon, J., Bleuse, J., Malik, N. S., Bazin, M., Jaffrennou, P., Gregersen, N., et al. (2010). A highly efficient single-photon source based on a quantum dot in a photonic nanowire. *Nature Photonics*, *4*, 174–177.
- Colombo, C., Heibeta, M., Gratzel, M., & Fontcuberta i Morral, A. (2009). Gallium arsenide p-i-n radial structures for photovoltaic applications. *Applied Physics Letters*, *94*, 173108.
- Czaban, J. A., Thompson, D. A., & Lapierre, R. R. (2008). GaAs core–shell nanowires for photovoltaic applications. *Nano Letters*, *9*, 148–154.
- Dai, X., Dayeh, S. A., Veeramuthu, V., Larrue, A., Wang, J., Su, H., et al. (2011). Tailoring the vapor–liquid–solid growth toward the self-assembly of GaAs nanowire junctions. *Nano Letters*, *11*, 4947–4952.
- Dalacu, D., Kam, A., Austing, D. G., & Poole, P. J. (2013). Droplet dynamics in controlled InAs nanowire interconnections. *Nano Letters*, *13*, 2676–2681.
- Dalacu, D., Kam, A., Guy Austing, D., Wu, X., Lapointe, J., Aers, G. C., et al. (2009). Selective-area vapour–liquid–solid growth of InP nanowires. *Nanotechnology*, *20*, 395602.
- Davydok, A., Rieger, T., Biermanns, A., Saqib, M., Grap, T., Lepsa, M. I., et al. (2013). Alloy formation during molecular beam epitaxy growth of Si-doped InAs nanowires on GaAs [111]B. *Journal of Applied Crystallography*, *46*, 893–897.
- Dayeh, S. A. (2010). Electron transport in indium arsenide nanowires. *Semiconductor Science and Technology*, *25*, 024004.
- Dayeh, S. A., Aplin, D. P. R., Zhou, X., Yu, P. K. L., Yu, E. T., & Wang, D. (2007). High electron mobility InAs nanowire field-effect transistors. *Small*, *3*, 326–332.
- Dayeh, S. A., Chen, P., Jing, Y., Yu, E. T., Lau, S. S., & Wang, D. (2008). Integration of vertical InAs nanowire arrays on insulator-on-silicon for electrical isolation. *Applied Physics Letters*, *93*, 203109.
- Dayeh, S. A., Hua Liu, X., Dai, X., Yu Huang, J., Picraux, S. T., & Soci, C. (2012). Rocking chair defect generation in nanowire growth. *Applied Physics Letters*, *101*, 053121.
- Dayeh, S. A., & Picraux, S. T. (2010). Direct observation of nanosize effects in Ge semiconductor nanowire growth. *Nano Letters*, *10*, 4032–4039.
- Dayeh, S. A., Soci, C., Bao, X.-Y., & Wang, D. (2009). Advances in the synthesis of InAs and GaAs nanowires for electronic applications. *Nano Today*, *4*, 347–358.
- Dayeh, S. A., Soci, C., Yu, P. K. L., Yu, E. T., & Wang, D. (2007a). Influence of surface states on the extraction of transport parameters from InAs nanowire field effect transistors. *Applied Physics Letters*, *90*, 162112.

- Dayeh, S. A., Soci, C., Yu, P. K. L., Yu, E. T., & Wang, D. (2007b). Transport properties of InAs nanowire field effect transistors: the effects of surface states. *Journal of Vacuum Science & Technology B: Microelectronics and Nanometer Structures*, 25, 1432.
- Dayeh, S. A., Susac, D., Kavanagh, K. L., Yu, E. T., & Wang, D. (2008). Field dependent transport properties in InAs nanowire field effect transistors. *Nano Lett*, 8, 3114–3119.
- Dayeh, S. A., Susac, D., Kavanagh, K. L., Yu, E. T., & Wang, D. (2009). Structural and room-temperature transport properties of zinc blende and wurtzite InAs nanowires. *Advanced Functional Materials*, 19, 2102–2108.
- Dayeh, S. A., Yu, E. T., & Wang, D. (2007c). Growth of InAs nanowires on SiO₂ substrates: nucleation, evolution, and the role of Au nanoparticles. *Journal of Physical Chemistry C*, 111, 13331–13336.
- Dayeh, S. A., Yu, E. T., & Wang, D. (2007d). III–V nanowire growth mechanism: V/III ratio and temperature effects. *Nano Letters*, 7, 2486–2490.
- Dayeh, S. A., Yu, E. T., & Wang, D. (2009). Transport coefficients of InAs nanowires as a function of diameter. *Small*, 5, 77–81.
- De, A., & Pryor, C. E. (2010). Predicted band structures of III-V semiconductors in the wurtzite phase. *Physical Review B*, 81, 155210.
- Dey, A. W., Borg, B. M., Ganjipour, B., Ek, M., Dick, K. A., Lind, E., et al. (2013). High-current GaSb/InAs(Sb) nanowire tunnel field-effect transistors. *IEEE Electron Device Letters*, 34, 211–213.
- Dey, A. W., Svensson, J., Ek, M., Lind, E., Thelander, C., & Wernersson, L.-E. (2013). Combining axial and radial nanowire heterostructures: radial Esaki diodes and tunnel field-effect transistors. *Nano Letters*, 13, 5919–5924.
- Dey, A. W., Thelander, C., Lind, E., Dick, K. A., Borg, B. M., Borgstrom, M., et al. (2012). High-performance InAs nanowire MOSFETs. *Electron Device Letters*, IEEE, 33, 791–793.
- Dheeraj, D. L., Munshi, A. M., Christoffersen, O. M., Kim, D. C., Signorello, G., Riel, H., et al. (2013). Comparison of Be-doped GaAs nanowires grown by Au- and Ga-assisted molecular beam epitaxy. *Journal of Crystal Growth*, 378, 532–536.
- Dheeraj, D. L., Patriarche, G., Zhou, H., Hoang, T. B., Moses, A. F., Grønsberg, S., et al. (2008). Growth and characterization of wurtzite GaAs nanowires with defect-free zinc blende GaAsSb inserts. *Nano Letters*, 8, 4459–4463.
- Dick, K. A., Bolinsson, J., Borg, B. M., & Johansson, J. (2012). Controlling the abruptness of axial heterojunctions in III-V nanowires: beyond the reservoir effect. *Nano Letters*, 12, 3200–3206.
- Dick, K. A., Caroff, P., Bolinsson, J., Messing, M. E., Johansson, J., Deppert, K., et al. (2010). Control of III–V nanowire crystal structure by growth parameter tuning. *Semiconductor Science and Technology*, 25, 024009.
- Dick, K. A., Deppert, K., Larsson, M. W., Martensson, T., Seifert, W., Wallenberg, L. R., et al. (2004). Synthesis of branched “nanotrees” by controlled seeding of multiple branching events. *Nature Materials*, 3, 380–384.
- Dick, K. A., Deppert, K., Mårtensson, T., Mandl, B., Samuelson, L., & Seifert, W. (2005). Failure of the vapor–liquid–solid mechanism in Au-assisted MOVPE growth of InAs nanowires. *Nano Letters*, 5, 761–764.
- Dick, K. A., Deppert, K., Samuelson, L., Wallenberg, L. R., & Ross, F. M. (2008). Control of GaP and GaAs nanowire morphology through particle and substrate chemical modification. *Nano Letters*, 8, 4087–4091.
- Dick, K. A., Thelander, C., Samuelson, L., & Caroff, P. (2010). Crystal phase engineering in single InAs nanowires. *Nano Letters*, 10, 3494–3499.

- Duan, X., Huang, Y., Cui, Y., Wang, J., & Lieber, C. M. (2001). Indium phosphide nanowires as building blocks for nanoscale electronic and optoelectronic devices. *Nature*, *409*, 66–69.
- Duan, X., Wang, J., & Lieber, C. M. (2000). Synthesis and optical properties of gallium arsenide nanowires. *Applied Physics Letters*, *76*, 1116–1118.
- Dubrovskii, V. G., & Sibirev, N. V. (2008). Growth thermodynamics of nanowires and its application to polytypism of zinc blende III-V nanowires. *Physical Review B*, *77*, 035414.
- Dubrovskii, V. G., Sibirev, N. V., Harmand, J. C., & Glas, F. (2008). Growth kinetics and crystal structure of semiconductor nanowires. *Physical Review B*, *78*, 235301.
- Du, S., Burgess, T., Gault, B., Gao, Q., Bao, P., Li, L., et al. (2013). Quantitative dopant distributions in GaAs nanowires using atom probe tomography. *Ultramicroscopy*, *132*, 186–192.
- Dufouleur, J., Colombo, C., Garma, T., Ketterer, B., Uccelli, E., Nicotra, M., et al. (2010). P-doping mechanisms in catalyst-free gallium arsenide nanowires. *Nano Letters*, *10*, 1734–1740.
- Ercolani, D., Rossi, F., Li, A., Roddaro, S., Grillo, V., Salvati, G., et al. (2009). InAs/InSb nanowire heterostructures grown by chemical beam epitaxy. *Nanotechnology*, *20*, 505605.
- Ertekin, E., Greaney, P. A., Chrzan, D. C., & Sands, T. D. (2005). Equilibrium limits of coherency in strained nanowire heterostructures. *Journal of Applied Physics*, *97*, 114325.
- Fang, Z. M., Ma, K. Y., Jaw, D. H., Cohen, R. M., & Stringfellow, G. B. (1990). Photoluminescence of InSb, InAs, and InAsSb grown by organometallic vapor phase epitaxy. *Journal of Applied Physics*, *67*, 7034–7039.
- Fang, L., Zhao, X., Chiu, Y.-H., Ko, D., Reddy, K. M., Lemberger, T. R., et al. (2011). Comprehensive control of optical polarization anisotropy in semiconducting nanowires. *Applied Physics Letters*, *99*, 141101.
- Fauzia, J., Vincenzo, G., Silvia, R., & Faustino, M. (2008). Self-catalyzed growth of GaAs nanowires on cleaved Si by molecular beam epitaxy. *Nanotechnology*, *19*, 275711.
- Fontcuberta I Morral, A., Colombo, C., Abstreiter, G., Arbiol, J., & Morante, J. R. (2008). Nucleation mechanism of gallium-assisted molecular beam epitaxy growth of gallium arsenide nanowires. *Applied Physics Letters*, *92*, 063112–063112-3.
- Fontcuberta I Morral, A., Spirkoska, D., Arbiol, J., Heigoldt, M., Morante, J. R., & Abstreiter, G. (2008). Prismatic quantum heterostructures synthesized on molecular-beam epitaxy GaAs nanowires. *Small*, *4*, 899–903.
- Ford, A. C., Chuang, S., Ho, J. C., Chueh, Y.-L., Fan, Z., & Javey, A. (2010). Patterned p-doping of InAs nanowires by gas-phase surface diffusion of Zn. *Nano Letters*, *10*, 509–513.
- Fortuna, S. A., & Li, X. (2009). GaAs MESFET with a high-mobility self-assembled planar nanowire channel. *Electron Device Letters*, *IEEE*, *30*, 593–595.
- Fortuna, S. A., & Li, X. (2010). Metal-catalyzed semiconductor nanowires: a review on the control of growth directions. *Semiconductor Science and Technology*, *25*, 024005.
- Fortuna, S. A., Wen, J., Chun, I. S., & Li, X. (2008). Planar GaAs nanowires on GaAs (100) substrates: self-aligned, nearly twin-defect free, and transfer-printable. *Nano Letters*, *8*, 4421–4427.
- Foster, A. P., & Wilson, L. R. (2013). Design parameters for nanowire-planar tandem solar cells. *Physica Status Solidi (A)*, *210*, 425–429.
- Friedler, I., Lalanne, P., Hugonin, J. P., Claudon, J., Gérard, J. M., Beveratos, A., et al. (2008). Efficient photonic mirrors for semiconductor nanowires. *Optics Letters*, *33*, 2635–2637.
- Friedler, I., Sauvan, C., Hugonin, J. P., Lalanne, P., Claudon, J., & Gérard, J. M. (2009). Solid-state single photon sources: the nanowire antenna. *Optics Express*, *17*, 2095–2110.
- Gallo, E. M., Chen, G., Currie, M., McGuckin, T., Prete, P., Lovergine, N., et al. (2011). Picosecond response times in GaAs/AlGaAs core/shell nanowire-based photodetectors. *Applied Physics Letters*, *98*, 241113.

- Gamalski, A. D., Tersoff, J., Sharma, R., Ducati, C., & Hofmann, S. (2010). Formation of metastable liquid catalyst during subeutectic growth of germanium nanowires. *Nano Letters*, *10*, 2972–2976.
- Ganjipour, B., Ek, M., Mattias Borg, B., Dick, K. A., Pistol, M.-E., Wernersson, L.-E., et al. (2012). Carrier control and transport modulation in GaSb/InAsSb core/shell nanowires. *Applied Physics Letters*, *101*.
- Ganjipour, B., Nilsson, H. A., Mattias Borg, B., Wernersson, L.-E., Samuelson, L., Xu, H. Q., et al. (2011). GaSb nanowire single-hole transistor. *Applied Physics Letters*, *99*, 262104.
- Ganjipour, B., Wallentin, J., Borgström, M. T., Samuelson, L., & Thelander, C. (2012). Tunnel field-effect transistors based on InP-GaAs heterostructure nanowires. *ACS Nano*, *6*, 3109–3113.
- Garnett, E. C., Brongersma, M. L., Cui, Y., & McGehee, M. D. (2011). Nanowire solar cells. *Annual Review of Materials Research*, *41*, 269–295.
- Ghosh, S. C., Kruse, P., & Lapierre, R. R. (2009). The effect of GaAs(100) surface preparation on the growth of nanowires. *Nanotechnology*, *20*, 115602.
- Givargizov, E. I. (1975). Fundamental aspects of VLS growth. *Journal of Crystal Growth*, *31*, 20–30.
- Glas, F. (2006). Critical dimensions for the plastic relaxation of strained axial heterostructures in free-standing nanowires. *Physical Review B*, *74*, 121302.
- Glas, F., Harmand, J.-C., & Patriarche, G. (2007). Why does wurtzite form in nanowires of III-V zinc blende semiconductors? *Physical Review Letters*, *99*, 146101.
- Glas, F., Patriarche, G., & Harmand, J. C. (2010). Growth, structure and phase transitions of epitaxial nanowires of III-V semiconductors. *Journal of Physics: Conference Series*, *209*, 012002.
- Goto, H., Nosaki, K., Tomioka, K., Hara, S., Hiruma, K., Motohisa, J., et al. (2009). Growth of core-shell InP nanowires for photovoltaic application by selective-area metal organic vapor phase epitaxy. *Applied Physics Express*, *2*, 035004.
- Grange, R., Brönstrup, G., Sergeev, A., Richter, J., Pertsch, T., Tünnermann, A., et al. (2012). In P. O. Spie (Ed.), *Imaging of waveguiding and scattering interferences in individual GaAs nanowires via second-harmonic generation* (pp. 84241J–84246J). SPIE.
- Gudiksen, M. S., Lauhon, L. J., Wang, J., Smith, D. C., & Lieber, C. M. (2002). Growth of nanowire superlattice structures for nanoscale photonics and electronics. *Nature*, *415*, 617–620.
- Gudiksen, M. S., Wang, J., & Lieber, C. M. (2001). Synthetic control of the diameter and length of single crystal semiconductor nanowires. *The Journal of Physical Chemistry B*, *105*, 4062–4064.
- Gudiksen, M. S., Wang, J., & Lieber, C. M. (2002). Size-dependent photoluminescence from single indium phosphide nanowires. *The Journal of Physical Chemistry B*, *106*, 4036–4039.
- Gutsche, C., Lysov, A., Braam, D., Regolin, I., Keller, G., Li, Z.-A., et al. (2012). n-GaAs/InGaP/p-GaAs core-multishell nanowire diodes for efficient light-to-current conversion. *Advanced Functional Materials*, *22*, 929–936.
- Hamano, T., Hirayama, H., & Aoyagi, Y. (1997). New technique for fabrication of two-dimensional photonic bandgap crystals by selective epitaxy. *Japanese Journal of Applied Physics*, *36*, L286–L288.
- Hannah, J. J., Callum, J. D., Qiang, G., Tan, H. H., Chennupati, J., James, L.-H., et al. (2013). Electronic properties of GaAs, InAs and InP nanowires studied by terahertz spectroscopy. *Nanotechnology*, *24*, 214006.

- Han, N., Wang, F., Yip, S., Hou, J. J., Xiu, F., Shi, X., et al. (2012). GaAs nanowire Schottky barrier photovoltaics utilizing Au–Ga alloy catalytic tips. *Applied Physics Letters*, *101*, 013105.
- Haraguchi, K., Katsuyama, T., & Hiruma, K. (1994). Polarization dependence of light emitted from GaAs p-n junctions in quantum wire crystals. *Journal of Applied Physics*, *75*, 4220–4225.
- Harmand, J. C., Patriarche, G., Pere-Laperne, N., Merat-Combes, M. N., Travers, L., & Glas, F. (2005). Analysis of vapor-liquid-solid mechanism in Au-assisted GaAs nanowire growth. *Applied Physics Letters*, *87*, 203101–203101-3.
- Hattori, T., Aiba, T., Iijima, E., Okube, Y., Nohira, H., Tate, N., et al. (1996). Initial stage of oxidation of hydrogen-terminated silicon surfaces. *Applied Surface Science*, *104–105*, 323–328.
- Heigoldt, M., Arbiol, J., Spirkoska, D., Rebled, J. M., Conesa-BOJ, S., Abstreiter, G., et al. (2009). Long range epitaxial growth of prismatic heterostructures on the facets of catalyst-free GaAs nanowires. *Journal of Materials Chemistry*, *19*, 840–848.
- Heinrich, J., Huggenberger, A., Heindel, T., Reitzenstein, S., Höfling, S., Worschech, L., et al. (2010). Single photon emission from positioned GaAs/AlGaAs photonic nanowires. *Applied Physics Letters*, *96*, 211117.
- Heiss, M., Fontana, Y., Gustafsson, A., Wüst, G., Magen, C., O’regan, D. D., et al. (2013). Self-assembled quantum dots in a nanowire system for quantum photonics. *Nature Materials*, *12*, 439–444.
- Heiss, M., & Fontcuberta i Morral, A. (2011). Fundamental limits in the external quantum efficiency of single nanowire solar cells. *Applied Physics Letters*, *99*, 263102.
- Himpsel, F. J., Mcfeely, F. R., Taleb-Ibrahimi, A., Yarmoff, J. A., & Hollinger, G. (1988). Microscopic structure of the SiO₂/Si interface. *Physical Review B*, *38*, 6084–6096.
- Hiruma, K., Yazawa, M., Katsuyama, T., Ogawa, K., Haraguchi, K., Koguchi, M., et al. (1995). Growth and optical properties of nanometer-scale GaAs and InAs whiskers. *Journal of Applied Physics*, *77*, 447–462.
- Hisamoto, D., Lee, W.-C., Kedzierski, J., Takeuchi, H., Asano, K., Kuo, C., et al. (2000). FinFET—A self-aligned double-gate MOSFET scalable to 20 nm. *IEEE Transactions on Electron Devices*, *47*, 2320–2325.
- Hjort, M., Wallentin, J., Timm, R., Zakharov, A. A., Andersen, J. N., Samuelson, L., et al. (2011). Doping profile of InP nanowires directly imaged by photoemission electron microscopy. *Applied Physics Letters*, *99*, 233113.
- Hoang, T. B., Moses, A. F., Zhou, H. L., Dheeraj, D. L., Fimland, B. O., & Weman, H. (2009). Observation of free exciton photoluminescence emission from single wurtzite GaAs nanowires. *Applied Physics Letters*, *94*, 133105.
- Ho, J. C., Ford, A. C., Chueh, Y.-L., Leu, P. W., Ergen, O., Takei, K., et al. (2009). Nanoscale doping of InAs via sulfur monolayers. *Applied Physics Letters*, *95*, 072108.
- Holm, J. V., Jorgensen, H. I., Krogstrup, P., Nygard, J., Liu, H., & Aagesen, M. (2013). Surface-passivated GaAsP single-nanowire solar cells exceeding 10% efficiency grown on silicon. *Nature Communications*, *4*, 1498.
- Hong, Y. J., Lee, W. H., Wu, Y., Ruoff, R. S., & Fukui, T. (2012). van der Waals epitaxy of InAs nanowires vertically aligned on single-layer graphene. *Nano Letters*, *12*, 1431–1436.
- Hua, B., Motohisa, J., Ding, Y., Hara, S., & Fukui, T. (2007). Characterization of Fabry-Pérot microcavity modes in GaAs nanowires fabricated by selective-area metal organic vapor phase epitaxy. *Applied Physics Letters*, *91*, 131112.
- Hua, B., Motohisa, J., Kobayashi, Y., Hara, S., & Fukui, T. (2008). Single GaAs/GaAsP coaxial core–shell nanowire lasers. *Nano Letters*, *9*, 112–116.

- Huang, H., Ren, X., Ye, X., Guo, J., Wang, Q., Yang, Y., et al. (2010). Growth of stacking-faults-free zinc blende GaAs nanowires on Si substrate by using AlGaAs/GaAs buffer layers. *Nano Letters*, *10*, 64–68.
- Hu, S., Chi, C.-Y., Fountaine, K. T., Yao, M., Atwater, H. A., Dapkus, P. D., et al. (2013). Optical, electrical, and solar energy-conversion properties of gallium arsenide nanowire-array photoanodes. *Energy & Environmental Science*, *6*, 1879–1890.
- Hyun, J. K., Zhang, S., & Lauhon, L. J. (2013). Nanowire heterostructures. *Annual Review of Materials Research*, *43*, 451–479.
- Ihn, S.-G., Ryu, M.-Y., & Song, J.-I. (2010). Optical properties of undoped, Be-doped, and Si-doped wurtzite-rich GaAs nanowires grown on Si substrates by molecular beam epitaxy. *Solid State Communications*, *150*, 729–733.
- Ihn, S.-G., Song, J.-I., Kim, Y.-H., & Yong Lee, J. (2006). GaAs nanowires on Si substrates grown by a solid source molecular beam epitaxy. *Applied Physics Letters*, *89*, 053106–053106-3.
- Ikejiri, K., Kitauchi, Y., Tomioka, K., Motohisa, J., & Fukui, T. (2011). Zinc blende and wurtzite crystal phase mixing and transition in indium phosphide nanowires. *Nano Letters*, *11*, 4314–4318.
- Ikejiri, K., Noborisaka, J., Hara, S., Motohisa, J., & Fukui, T. (2007). Mechanism of catalyst-free growth of GaAs nanowires by selective area MOVPE. *Journal of Crystal Growth*, *298*, 616–619.
- Ikejiri, K., Sato, T., Yoshida, H., Hiruma, K., Motohisa, J., Hara, S., et al. (2008). Growth characteristics of GaAs nanowires obtained by selective area metal–organic vapour-phase epitaxy. *Nanotechnology*, *19*, 265604.
- Ingle, S., Aella, P., Manandhar, P., Chikkannanavar, S. B., Akhadvov, E. A., Smith, D. J., et al. (2008). Ex situ doping of silicon nanowires with boron. *Journal of Applied Physics*, *103*, 104302.
- Ionescu, A. M., & Riel, H. (2011). Tunnel field-effect transistors as energy-efficient electronic switches. *Nature*, *479*, 329–337.
- Jeppsson, M., Dick, K. A., Nilsson, H. A., Sköld, N., Wagner, J. B., Caroff, P., et al. (2008). Characterization of GaSb nanowires grown by MOVPE. *Journal of Crystal Growth*, *310*, 5119–5122.
- Jeppsson, M., Dick, K. A., Wagner, J. B., Caroff, P., Deppert, K., Samuelson, L., et al. (2008). GaAs/GaSb nanowire heterostructures grown by MOVPE. *Journal of Crystal Growth*, *310*, 4115–4121.
- Jiang, N., Gao, Q., Parkinson, P., Wong-Leung, J., Mokkapatil, S., Breuer, S., et al. (2013). Enhanced minority carrier lifetimes in GaAs/AlGaAs core–shell nanowires through shell growth optimization. *Nano Letters*, *13*, 5135–5140.
- Jiang, X., Tian, B., Xiang, J., Qian, F., Zheng, G., Wang, H., et al. (2011). Rational growth of branched nanowire heterostructures with synthetically encoded properties and function. *Proceedings of the National Academy of Sciences*, *108*, 12212–12216.
- Jiang, X., Xiong, Q., Nam, S., Qian, F., Li, Y., & Lieber, C. M. (2007). InAs/InP radial nanowire heterostructures as high electron mobility devices. *Nano Letters*, *7*, 3214–3218.
- Johansson, J., Dick, K. A., Caroff, P., Messing, M. E., Bolinsson, J., Deppert, K., et al. (2010). Diameter dependence of the wurtzite-zinc blende transition in InAs nanowires. *Journal of Physical Chemistry C*, *114*, 3837–3842.
- Johansson, J., Karlsson, L. S., Patrik, T., Svensson, C., Mårtensson, T., Wacaser, B. A., et al. (2006). Structural properties of $\langle 111 \rangle$ B-oriented III–V nanowires. *Nature Materials*, *5*, 574–580.

- Johnson, S. G., Mekis, A., Shanhui, F., & Joannopoulos, J. D. (2001). Molding the flow of light. *Computing in Science & Engineering*, 3, 38–47.
- Joyce, B. D., & Baldrey, J. A. (1962). Selective epitaxial deposition of silicon. *Nature*, 195, 485–486.
- Joyce, H. J., Gao, Q., Hoe Tan, H., Jagadish, C., Kim, Y., Zou, J., et al. (2011). III–V semiconductor nanowires for optoelectronic device applications. *Progress in Quantum Electronics*, 35, 23–75.
- Joyce, H. J., Gao, Q., Tan, H. H., Jagadish, C., Kim, Y., Fickenscher, M. A., et al. (2008). High purity GaAs nanowires free of planar defects: growth and characterization. *Advanced Functional Materials*, 18, 3794–3800.
- Jung-Hyun, K., Qiang, G., Joyce, H. J., Tan, H. H., Jagadish, C., Yong, K., et al. (2010). Improvement of morphology, structure, and optical properties of GaAs nanowires grown on Si substrates. In *Nanotechnology (IEEE-NANO), 2010 10th IEEE conference on, 17–20 August 2010* (pp. 470–473).
- Kang, J. H., Cohen, Y., Ronen, Y., Heiblum, M., Buczko, R., Kacman, P., et al. (2013). Crystal structure and transport in merged InAs nanowires MBE grown on (001) InAs. *Nano Letters*, 13, 5190–5196.
- Kang, J. H., Gao, Q., Joyce, H. J., Tan, H. H., Jagadish, C., Kim, Y., et al. (2010). Novel growth and properties of GaAs nanowires on Si substrates. *Nanotechnology*, 21, 035604.
- Karlsson, L. S., Dick, K. A., Wagner, J. B., Malm, J.-O., Deppert, K., Samuelson, L., et al. (2007). Understanding the 3D structure of $\{GaAs\langle 111\rangle B\}$ nanowires. *Nanotechnology*, 18, 485717.
- Katsuhiko, T., Yasunori, K., Junichi, M., Shinjiroh, H., & Takashi, F. (2009). Selective-area growth of vertically aligned GaAs and GaAs/AlGaAs core–shell nanowires on Si(111) substrate. *Nanotechnology*, 20, 145302.
- Kayes, B. M., Atwater, H. A., & Lewis, N. S. (2005). Comparison of the device physics principles of planar and radial p-n junction nanorod solar cells. *Journal of Applied Physics*, 97, 114302.
- Ketterer, B., Heiss, M., Livrozet, M. J., Rudolph, A., Reiger, E., Morral, F. I., et al. (2011). Determination of the band gap and the split-off band in wurtzite GaAs using Raman and photoluminescence excitation spectroscopy. *Physical Review B*, 83, 125307.
- Ketterer, B., Uccelli, E., & Morral, A. F. I. (2012). Mobility and carrier density in p-type GaAs nanowires measured by transmission Raman spectroscopy. *Nanoscale*, 4, 1789–1793.
- Khorenko, V., Regolin, I., Neumann, S., Prost, W., Tegude, F.-J., & Wiggers, H. (2004). Photoluminescence of GaAs nanowhiskers grown on Si substrate. *Applied Physics Letters*, 85, 6407–6408.
- Kim, D. C., Ahtapodov, L., Boe, A. B., Choi, J. W., Ji, H., Kim, G. T., et al. (2011). Photocurrent spectroscopy of single wurtzite GaAs nanowires. *AIP Conference Proceedings*, 1399, 429–430.
- Kim, D. C., Dheeraj, D. L., Fimland, B. O., & Weman, H. (2013). Polarization dependent photocurrent spectroscopy of single wurtzite GaAs/AlGaAs core-shell nanowires. *Applied Physics Letters*, 102, 142107.
- Kobayashi, N. P., Logeeswaran, V. J., Xuema, L., Islam, M. S., Straznicki, J., Shih-Yuan, W., et al. (2007). Indium phosphide nanowire photoconductors on non-single crystalline silicon-based platform. In *Nanotechnology, 2007. IEEE-nano 2007. 7th IEEE conference on, 2–5 August 2007* (pp. 1339–1343).
- Kobl Müller, G., Hertenberger, S., Vizbaras, K., Bichler, M., Bao, F., Zhang, J. P., et al. (2010). Self-induced growth of vertical free-standing InAs nanowires on Si(111) by molecular beam epitaxy. *Nanotechnology*, 21, 365602.

- Kodambaka, S., Tersoff, J., Reuter, M. C., & Ross, F. M. (2007). Germanium nanowire growth below the eutectic temperature. *Science*, *316*, 729–732.
- Koguchi, M., Kakibayashi, H., Yazawa, M., Hiruma, K., & Katsuyama, T. (1992). Crystal structure change of GaAs and InAs whiskers from zinc-blende to wurtzite type. *Japanese Journal of Applied Physics*, *31*, 2061–2065.
- Krishnamachari, U., Borgstrom, M., Ohlsson, B. J., Panev, N., Samuelson, L., Seifert, W., et al. (2004). Defect-free InP nanowires grown in [001] direction on InP (001). *Applied Physics Letters*, *85*, 2077–2079.
- Krogstrup, P., Jørgensen, H. I., Heiss, M., Demichel, O., Holm, J. V., Aagesen, M., et al. (2013). Single-nanowire solar cells beyond the Shockley-Queisser limit. *Nature Photonics*, *7*, 306–310.
- Lapierre, R. R. (2011a). Numerical model of current-voltage characteristics and efficiency of GaAs nanowire solar cells. *Journal of Applied Physics*, *109*, 034311.
- Lapierre, R. R. (2011b). Theoretical conversion efficiency of a two-junction III-V nanowire on Si solar cell. *Journal of Applied Physics*, *110*, 014310.
- Lapierre, R. R., Chia, A. C. E., Gibson, S. J., Haapamaki, C. M., Boulanger, J., Yee, R., et al. (2013). III–V nanowire photovoltaics: review of design for high efficiency. *Physica Status Solidi (RRL) – Rapid Research Letters*, *7*, 815–830.
- Larue, A., Wilhelm, C., Vest, G., Combr e, S., De Rossi, A., & Soci, C. (2012). Monolithic integration of III-V nanowire with photonic crystal microcavity for vertical light emission. *Optics Express*, *20*, 7758–7770.
- Lee, C. C., Wang, C. Y., & Matijasevic, G. (1993). Au-In bonding below the eutectic temperature. *IEEE Transactions on Components, Hybrids, and Manufacturing Technology*, *16*, 311–316.
- Lin, H.-M., Chen, Y.-L., Yang, J., Liu, Y.-C., Yin, K.-M., Kai, J.-J., et al. (2003). Synthesis and characterization of core–shell GaP@GaN and GaN@GaP nanowires. *Nano Letters*, *3*, 537–541.
- Lind, E., Persson, A. I., Samuelson, L., & Wernersson, L.-E. (2006). Improved subthreshold slope in an InAs nanowire heterostructure field-effect transistor. *Nano Lett*, *6*, 1842–1846.
- Littler, C. L., & Seiler, D. G. (1985). Temperature dependence of the energy gap of InSb using nonlinear optical techniques. *Applied Physics Letters*, *46*, 986–988.
- Liu, B. D., Bando, Y., Tang, C. C., Golberg, D., Xie, R. G., & Sekiguchi, T. (2005). Synthesis and optical study of crystalline GaP nanoflowers. *Applied Physics Letters*, *86*, 083107.
- Lugani, L., Ercolani, D., Sorba, L., Sibirev, N. V., Timofeeva, M. A., & Dubrovskii, V. G. (2012). Modeling of InAs–InSb nanowires grown by Au-assisted chemical beam epitaxy. *Nanotechnology*, *23*, 095602.
- Lysov, A., Gutsche, C., Offer, M., Regolin, I., Prost, W., & Tegude, F. J. (2011). Spatially resolved photovoltaic performance of axial GaAs nanowire pn-diodes. In *Device research conference (DRC), 2011 69th annual, 20–22 June 2011* (pp. 53–54).
- Madelung, O. (2004). *Semiconductors: Data handbook*. Springer.
- Maharjan, A., Pemasiri, K., Kumar, P., Wade, A., Smith, L. M., Jackson, H. E., et al. (2009). Room temperature photocurrent spectroscopy of single zincblende and wurtzite InP nanowires. *Applied Physics Letters*, *94*, 193115.
- Makhonin, M. N., Foster, A. P., Krysa, A. B., Fry, P. W., Davies, D. G., Grange, T., et al. (2013). Homogeneous array of nanowire-embedded quantum light emitters. *Nano Letters*, *13*, 861–865.
- Manasevit, H. M. (1968). Single-Crystal gallium arsenide on insulating substrates. *Applied Physics Letters*, *12*, 156–159.

- Mandl, B., Stangl, J., Mårtensson, T., Mikkelsen, A., Eriksson, J., Karlsson, L. S., et al. (2006). Au-free epitaxial growth of InAs nanowires. *Nano Letters*, 6, 1817–1821.
- Mariager, S. O., Sorensen, C. B., Aagesen, M., Nygård, J., Feidenhans'l, R., & Willmott, P. R. (2007). Facet structure of GaAs nanowires grown by molecular beam epitaxy. *Applied Physics Letters*, 91, 083106.
- Mårtensson, T., Svensson, C. P. T., Wacaser, B. A., Larsson, M. W., Seifert, W., Deppert, K., et al. (2004). Epitaxial III–V nanowires on silicon. *Nano Letters*, 4, 1987–1990.
- Maslov, A. V., & Ning, C. Z. (2003). Reflection of guided modes in a semiconductor nanowire laser. *Applied Physics Letters*, 83, 1237–1239.
- Maslov, A. V., & Ning, C. Z. (2004). Modal properties of semiconductor nanowires for laser applications. *Proceedings of SPIE*, 24–30.
- Mattila, M., Hakkarainen, T., Jiang, H., Kauppinen, E. I., & Lipsanen, H. (2007). Effect of substrate orientation on the catalyst-free growth of InP nanowires. *Nanotechnology*, 18, 155301.
- Mattila, M., Hakkarainen, T., Lipsanen, H., Jiang, H., & Kauppinen, E. I. (2006). Catalyst-free growth of In(As)P nanowires on silicon. *Applied Physics Letters*, 89, 063119–063119-3.
- Mattila, M., Hakkarainen, T., Mulo, M., & Lipsanen, H. (2006). Crystal-structure-dependent photoluminescence from InP nanowires. *Nanotechnology*, 17, 1580.
- Messing, M. E., Wong-Leung, J., Zanolli, Z., Joyce, H. J., Tan, H. H., Gao, Q., et al. (2011). Growth of straight InAs-on-GaAs nanowire heterostructures. *Nano Letters*, 11, 3899–3905.
- Mi, Z. (2009). III-V compound semiconductor nanostructures on silicon: epitaxial growth, properties, and applications in light emitting diodes and lasers. *Journal of Nanophotonics*, 3, 031602.
- Miao, X., & Li, X. (2011). Towards planar GaAs nanowire array high electron mobility transistor. In *Device research conference (DRC), 2011 69th annual, 20–22 June 2011* (pp. 115–116).
- Miederer, W., Ziegler, G., & Dotzer, R. (25 September, 1962). *Verfahren zum tiegfremigen Herstellen von Galliumarsenidstäben aus Galliumalkylen und Arsenverbindungen bei niedrigen Temperaturen*.
- Miederer, W., Ziegler, G., & Dotzer, R. (24 September, 1963). *Method of crucible-free production of gallium arsenide rods from alkyl galliums and arsenic compounds at low temperatures*.
- Mikkelsen, A., Ouattara, L., Davidsson, H., Lundgren, E., Sadowski, J., & Pacherova, O. (2004). Mn diffusion in Ga1–xMnxAs/GaAs superlattices. *Applied Physics Letters*, 85, 4660–4662.
- Mikkelsen, A., Skold, N., Ouattara, L., Borgstrom, M., Andersen, J. N., Samuelson, L., et al. (2004). Direct imaging of the atomic structure inside a nanowire by scanning tunnelling microscopy. *Nature Materials*, 3, 519–523.
- Mikkelsen, A., Sköld, N., Ouattara, L., & Lundgren, E. (2006). Nanowire growth and dopants studied by cross-sectional scanning tunnelling microscopy. *Nanotechnology*, 17, S362.
- Miller, O. D., Yablonovitch, E., & Kurtz, S. R. (2012). Strong internal and external luminescence as solar cells approach the Shockley-Queisser limit. *Photovoltaics, IEEE Journal of*, 2, 303–311.
- Minot, E. D., Kelkensberg, F., Van Kouwen, M., Van Dam, J. A., Kouwenhoven, L. P., Zwiller, V., et al. (2007). Single quantum dot nanowire LEDs. *Nano Letters*, 7, 367–371.
- Mishra, A., Titova, L. V., Hoang, T. B., Jackson, H. E., Smith, L. M., Yarrison-Rice, J. M., et al. (2007). Polarization and temperature dependence of photoluminescence from zincblende and wurtzite InP nanowires. *Applied Physics Letters*, 91, 263104.

- Moewe, M., Chuang, L. C., Crankshaw, S., Chase, C., & Chang-Hasnain, C. (2008). Atomically sharp catalyst-free wurtzite GaAs/AlGaAs nanoneedles grown on silicon. *Applied Physics Letters*, *93*, 023116.
- Mohammad, S. N. (2009). For nanowire growth, vapor-solid-solid (vapor-solid) mechanism is actually vapor-quasisolid-solid (vapor-quasiliquid-solid) mechanism. *The Journal of Chemical Physics*, *131*, 224702.
- Mohan, P., Motohisa, J., & Fukui, T. (2006). Fabrication of InP/InAs/InP core-multishell heterostructure nanowires by selective area metalorganic vapor phase epitaxy. *Applied Physics Letters*, *88*, 133105.
- Mohseni, P. K., Maunders, C., Botton, G. A., & Lapierre, R. R. (2007). GaP/GaAsP/GaP core-multishell nanowire heterostructures on (111) silicon. *Nanotechnology*, *18*, 445304.
- Morales, A. M., & Lieber, C. M. (1998). A laser ablation method for the synthesis of crystalline semiconductor nanowires. *Science*, *279*, 208–211.
- Motohisa, J., Noborisaka, J., Takeda, J., Inari, M., & Fukui, T. (2004). Catalyst-free selective-area MOVPE of semiconductor nanowires on (111)B oriented substrates. *Journal of Crystal Growth*, *272*, 180–185.
- Motohisa, J., Takeda, J., Inari, M., Noborisaka, J., & Fukui, T. (2004). Growth of GaAs/AlGaAs hexagonal pillars on GaAs (1 1 1)B surfaces by selective-area MOVPE. *Physica E: Low-dimensional Systems and Nanostructures*, *23*, 298–304.
- Müller, E. W., Panitz, J. A., & McLane, S. B. (1968). The atom-probe field ion microscope. *Review of Scientific Instruments*, *39*, 83–86.
- Munshi, A. M., Dheeraj, D. L., Fauske, V. T., Kim, D.-C., Van Helvoort, A. T. J., Fimland, B.-O., et al. (2012). Vertically aligned GaAs nanowires on graphite and few-layer graphene: generic model and epitaxial growth. *Nano Letters*, *12*, 4570–4576.
- Murayama, M., & Nakayama, T. (1994). Chemical trend of band offsets at wurtzite/zinc-blende heterocrystalline semiconductor interfaces. *Physical Review B*, *49*, 4710–4724.
- Muskens, O. L., Diedenhofen, S. L., Kaas, B. C., Algra, R. E., Bakkers, E. P. A. M., Gómez Rivas, J., et al. (2009). Large photonic strength of highly tunable resonant nanowire materials. *Nano Letters*, *9*, 930–934.
- Muskens, O. L., Rivas, J. G., Algra, R. E., Bakkers, E. P. A. M., & Lagendijk, A. (2008). Design of light scattering in nanowire materials for photovoltaic applications. *Nano Letters*, *8*, 2638–2642.
- Nakai, E., Yoshimura, M., Tomioka, K., & Fukui, T. (2013). GaAs/InGaP core-multishell nanowire-array-based solar cells. *Japanese Journal of Applied Physics*, *52*, 055002.
- Ng, K. W., Ko, W. S., Tran, T.-T. D., Chen, R., Nazarenko, M. V., Lu, F., et al. (2012). Unconventional growth mechanism for monolithic integration of III–V on silicon. *ACS Nano*, *7*, 100–107.
- Nguyen, P., Ng, H. T., & Meyyappan, M. (2005). Catalyst metal selection for synthesis of inorganic nanowires. *Advanced Materials*, *17*, 1773–1777.
- Nilsson, H. A., Caroff, P., Thelander, C., Larsson, M., Wagner, J. B., Wernersson, L.-E., et al. (2009). Giant, level-dependent g factors in InSb nanowire quantum dots. *Nano Letters*, *9*, 3151–3156.
- Ning, C. Z. (2010). Semiconductor nanolasers. *Physica Status Solidi (B)*, *247*, 774–788.
- Noborisaka, J., Motohisa, J., Hara, S., & Fukui, T. (2005). Fabrication and characterization of freestanding GaAs/AlGaAs core-shell nanowires and AlGaAs nanotubes by using selective-area metalorganic vapor phase epitaxy. *Applied Physics Letters*, *87*, 093109–093109-3.
- Novotny, C. J., & Yu, P. K. L. (2005). Vertically aligned, catalyst-free InP nanowires grown by metalorganic chemical vapor deposition. *Applied Physics Letters*, *87*, 203111–203111-3.

- Ohlsson, B. J., Björk, M. T., Persson, A. I., Thelander, C., Wallenberg, L. R., Magnusson, M. H., et al. (2002). Growth and characterization of GaAs and InAs nanowhiskers and InAs/GaAs heterostructures. *Physica E: Low-dimensional Systems and Nanostructures*, *13*, 1126–1130.
- Panev, N., Persson, A. I., Sköld, N., & Samuelson, L. (2003). Sharp exciton emission from single InAs quantum dots in GaAs nanowires. *Applied Physics Letters*, *83*, 2238–2240.
- Park, H. D., Prokes, S. M., Twigg, M. E., Ding, Y., & Wang, Z. L. (2007). Growth of high quality, epitaxial InSb nanowires. *Journal of Crystal Growth*, *304*, 399–401.
- Paul, R. K., Penchev, M., Zhong, J., Ozkan, M., Ghazinejad, M., Jing, X., et al. (2010). Chemical vapor deposition and electrical characterization of sub-10 nm diameter InSb nanowires and field-effect transistors. *Materials Chemistry and Physics*, *121*, 397–401.
- Pemasiri, K., Montazeri, M., Gass, R., Smith, L. M., Jackson, H. E., Yarrison-Rice, J., et al. (2009). Carrier dynamics and quantum confinement in type ii ZB-WZ InP nanowire homostructures. *Nano Letters*, *9*, 648–654.
- Pendyala, C., Vaddiraju, S., Kim, J. H., Jacinski, J., Chen, Z., & Sunkara, M. K. (2010). Self-nucleation and growth of group III-antimonide nanowires. *Semiconductor Science and Technology*, *25*, 024014.
- Perea, D. E., Allen, J. E., May, S. J., Wessels, B. W., Seidman, D. N., & Lauhon, L. J. (2006). Three-dimensional nanoscale composition mapping of semiconductor nanowires. *Nano Letters*, *6*, 181–185.
- Persano, A., Nabet, B., Taurino, A., Prete, P., Lovergine, N., & Cola, A. (2011). Polarization anisotropy of individual core/shell GaAs/AlGaAs nanowires by photocurrent spectroscopy. *Applied Physics Letters*, *98*, 153106.
- Persson, A. I., Fröberg, L. E., Jeppesen, S., Björk, M. T., & Samuelson, L. (2007). Surface diffusion effects on growth of nanowires by chemical beam epitaxy. *Journal of Applied Physics*, *101*, 034313.
- Persson, A. I., Larsson, M. W., Stenström, S., Ohlsson, B. J., Samuelson, L., & Wallenberg, L. R. (2004). Solid-phase diffusion mechanism for GaAs nanowire growth. *Nature Materials*, *3*, 677–681.
- Persson, A. I., Ohlsson, B. J., Jeppesen, S., & Samuelson, L. (2004). Growth mechanisms for GaAs nanowires grown in CBE. *Journal of Crystal Growth*, *272*, 167–174.
- Pettersson, H., Trägårdh, J., Persson, A. I., Landin, L., Hessman, D., & Samuelson, L. (2006). Infrared photodetectors in heterostructure nanowires. *Nano Letters*, *6*, 229–232.
- Plissard, S., Dick, K. A., Wallart, X., & Caroff, P. (2010). Gold-free GaAs/GaAsSb heterostructure nanowires grown on silicon. *Applied Physics Letters*, *96*, 121901.
- Plissard, S., Larrieu, G., Wallart, X., & Caroff, P. (2011). High yield of self-catalyzed GaAs nanowire arrays grown on silicon via gallium droplet positioning. *Nanotechnology*, *22*, 275602.
- Plissard, S. R., Slapak, D. R., Verheijen, M. A., Hocevar, M., Immink, G. W. G., Van Weperen, I., et al. (2012). From InSb nanowires to nanocubes: looking for the sweet spot. *Nano Letters*, *12*, 1794–1798.
- Plissard, S. R., Van Weperen, I., Car, D., Verheijen, M. A., Immink, G. W. G., Kammhuber, J., et al. (2013). Formation and electronic properties of InSb nanocrosses. *Nature Nanotechnology*, *8*, 859–864.
- Poole, P. J., Lefebvre, J., & Fraser, J. (2003). Spatially controlled, nanoparticle-free growth of InP nanowires. *Applied Physics Letters*, *83*, 2055–2057.
- Pratyush Das, K., Heinz, S., Mikael, T. B., Lynne, M. G., Chris, B., John, B., et al. (2013). Selective area growth of III–V nanowires and their heterostructures on silicon in

- a nanotube template: towards monolithic integration of nano-devices. *Nanotechnology*, *24*, 225304.
- Rehnstedt, C., Martensson, T., Thelander, C., Samuelson, L., & Wernersson, L. E. (2008). Vertical InAs nanowire wrap gate transistors on Si substrates. *Electron Devices, IEEE Transactions on*, *55*, 3037–3041.
- Reimer, M. E., Bulgarini, G., Akopian, N., Hocevar, M., Bavinck, M. B., Verheijen, M. A., et al. (2012). Bright single-photon sources in bottom-up tailored nanowires. *Nature Communications*, *3*, 737.
- Ren, S., Zhao, N., Crawford, S. C., Tambe, M., Bulović, V., & Gradecak, S. (2010). Heterojunction photovoltaics using GaAs nanowires and conjugated polymers. *Nano Letters*, *11*, 408–413.
- Riel, H., Moselund, K. E., Bessire, C., Bjork, M. T., Schenk, A., Ghoneim, H., et al. (2012). InAs-Si heterojunction nanowire tunnel diodes and tunnel FETs. Electron devices meeting (IEDM). In *2012 IEEE international, 10–13 December 2012* (pp. 16.6.1–16.6.4).
- Roddaro, S., Nilsson, K., Astromskas, G., Samuelson, L., Wernersson, L.-E., Karlström, O., et al. (2008). InAs nanowire metal-oxide-semiconductor capacitors. *Applied Physics Letters*, *92*, 253509.
- Roest, A. L., Verheijen, M. A., Wunnicke, O., Serafin, S., Wondergem, H., & Bakkers, E. P. A. M. (2006). Position-controlled epitaxial III–V nanowires on silicon. *Nanotechnology*, *17*, S271–S275.
- Rolland, C., Caroff, P., Coinon, C., Wallart, X., & Leturcq, R. (2013). Inhomogeneous Si-doping of gold-seeded InAs nanowires grown by molecular beam epitaxy. *Applied Physics Letters*, *102*, 223105.
- Ruda, H. E., & Shik, A. (2005). Polarization-sensitive optical phenomena in semiconducting and metallic nanowires. *Physical Review B*, *72*, 115308.
- Ruda, H. E., & Shik, A. (2007). Nonlinear optical phenomena in nanowires. *Journal of Applied Physics*, *101*, 034312.
- Sau, J. D., Clarke, D. J., & Tewari, S. (2011). Controlling non-Abelian statistics of Majorana fermions in semiconductor nanowires. *Physical Review B*, *84*, 094505.
- Saxena, D., Mokkapatil, S., Parkinson, P., Jiang, N., Gao, Q., Tan, H. H., et al. (2013). Optically pumped room-temperature GaAs nanowire lasers. *Nature Photonics*, *7*, 963–968.
- Schmidt, V., Senz, S., & Gösele, U. (2015). Diameter-dependent growth direction of epitaxial silicon nanowires. *Nano Letters*, *5*, 931–935.
- Schricker, A. D., Davidson, F. M., Wiacek, R. J., & Korgel, B. A. (2006). Space charge limited currents and trap concentrations in GaAs nanowires. *Nanotechnology*, *17*, 2681–2688.
- Schroer, M. D., & Petta, J. R. (2010). Correlating the nanostructure and electronic properties of InAs nanowires. *Nano Letters*, *10*, 1618–1622.
- Schwalbach, E. J., & Voorhees, P. W. (2009). Doping nanowires grown by the vapor-liquid-solid mechanism. *Applied Physics Letters*, *95*, 063105.
- Scofield, A. C., Kim, S.-H., Shapiro, J. N., Lin, A., Liang, B., Scherer, A., et al. (2011). Bottom-up photonic crystal lasers. *Nano Letters*, *11*, 5387–5390.
- Seifert, W., Borgström, M., Deppert, K., Dick, K. A., Johansson, J., Larsson, M. W., et al. (2004). Growth of one-dimensional nanostructures in MOVPE. *Journal of Crystal Growth*, *272*, 211–220.
- Shen, G., Bando, Y., Liu, B., Tang, C., & Golberg, D. (2006). Unconventional zigzag indium phosphide single-crystalline and twinned nanowires. *The Journal of Physical Chemistry B*, *110*, 20129–20132.

- Shin, J. C., Lee, A., Katal Mohseni, P., Kim, D. Y., Yu, L., Kim, J. H., et al. (2013). Wafer-scale production of uniform InAs_{1-y}P_y nanowire array on silicon for heterogeneous integration. *ACS Nano*, *7*, 5463–5471.
- Shi, W. S., Zheng, Y. F., Wang, N., Lee, C. S., & Lee, S. T. (2001). Synthesis and microstructure of gallium phosphide nanowires. *Journal of Vacuum Science & Technology B: Microelectronics and Nanometer Structures*, *19*, 1115.
- Shockley, W., & Queisser, H. J. (1961). Detailed balance limit of efficiency of p-n junction solar cells. *Journal of Applied Physics*, *32*, 510–519.
- Sladek, K., Klinger, V., Wensorra, J., Akabori, M., Hardtdegen, H., & Grützmacher, D. (2010). MOVPE of n-doped GaAs and modulation doped GaAs/AlGaAs nanowires. *Journal of Crystal Growth*, *312*, 635–640.
- Soci, C., Zhang, A., Bao, X. Y., Kim, H., Lo, Y., & Wang, D. L. (2010). Nanowire photodetectors. *Journal of Nanoscience and Nanotechnology*, *10*, 1430–1449.
- Soo-Ghang, I., & Jong-In, S. (2007). InAs nanowires on Si substrates grown by solid source molecular beam epitaxy. *Nanotechnology*, *18*, 355603.
- Soo-Ghang, I., Jong-In, S., Young-Hun, K., Yong Lee, J., & Il-Ho, A. (2007). Growth of GaAs nanowires on Si substrates using a molecular beam epitaxy. *Nanotechnology, IEEE Transactions on*, *6*, 384–389.
- Spirkoska, D., Abstreiter, G., & Morral, A. F. I. (2009). GaAs nanowires and related prismatic heterostructures. *Semiconductor Science and Technology*, *24*, 113001.
- Storm, K., Nylund, G., Borgstrom, M., Wallentin, J., Fath, C., Thelander, C., et al. (2011). Gate-induced Fermi level tuning in InP nanowires at efficiency close to the thermal limit. *Nano Letters*, *11*, 1127–1130.
- Storm, K., Nylund, G., Samuelson, L., & Micolich, A. P. (2011). Realizing lateral wrap-gated nanowire FETs: controlling gate length with chemistry rather than lithography. *Nano Letters*, *12*, 1–6.
- Sutter, E. A., & Sutter, P. W. (2010). Size-dependent phase diagram of nanoscale alloy drops used in Vapor–Liquid–Solid growth of semiconductor nanowires. *ACS Nano*, *4*, 4943–4947.
- Suyatin, D. B., Sun, J., Fuhrer, A., Wallin, D., Fröberg, L. E., Karlsson, L. S., et al. (2008). Electrical properties of self-assembled branched InAs nanowire junctions. *Nano Lett*, *8*, 1100–1104.
- Svensson, C. P. T., Seifert, W., Larsson, M. W., Wallenberg, L. R., Stangl, J., Bauer, G., et al. (2005). Epitaxially grown GaP/GaAs_{1-x}P_x/GaP double heterostructure nanowires for optical applications. *Nanotechnology*, *16*, 936.
- Svensson, C. P. T., Thomas, M., Johanna, T., Christina, L., Michael, R., Dan, H., et al. (2008). Monolithic GaAs/InGaP nanowire light emitting diodes on silicon. *Nanotechnology*, *19*, 305201.
- Tanaka, T., Tomioka, K., Hara, S., Motohisa, J., Sano, E., & Fukui, T. (2010). Vertical surrounding gate transistors using single InAs nanowires grown on Si substrates. *Applied Physics Express*, *3*, 025003.
- Tang, C., Bando, Y., Liu, Z., & Golberg, D. (2003). Synthesis and structure of InP nanowires and nanotubes. *Chemical Physics Letters*, *376*, 676–682.
- Tateno, K., Hibino, H., Gotoh, H., & Nakano, H. (2006). Vertical GaP nanowires arranged at atomic steps on Si(111) substrates. *Applied Physics Letters*, *89*, 033114.
- Tateno, K., Zhang, G., & Nakano, H. (2008). InP nanostructures formed in GaP-based nanowires grown on Si(1 1 1) substrates. *Journal of Crystal Growth*, *310*, 2966–2969.

- Tchernycheva, M., Rigutti, L., Jacopin, G., Bugallo, A. D. L., Lavenus, P., Julien, F. H., et al. (2012). Photovoltaic properties of GaAsP core-shell nanowires on Si(001) substrate. *Nanotechnology*, *23*, 265402.
- Tchernycheva, M., Travers, L., Patriarche, G., Glas, F., Harmand, J.-C., Cirlin, G. E., et al. (2007). Au-assisted molecular beam epitaxy of InAs nanowires: growth and theoretical analysis. *Journal of Applied Physics*, *102*, 094313.
- Thelander, C., Agarwal, P., Brongersma, S., Eymery, J., Feiner, L. F., Forchel, A., et al. (2006). Nanowire-based one-dimensional electronics. *Materials Today*, *9*, 28–35.
- Thelander, C., Björk, M. T., Larsson, M. W., Hansen, A. E., Wallenberg, L. R., & Samuelson, L. (2004). Electron transport in InAs nanowires and heterostructure nanowire devices. *Solid State Communications*, *131*, 573–579.
- Thelander, C., Caroff, P., Plissard, S. B., Dey, A. W., & Dick, K. A. (2011). Effects of crystal phase mixing on the electrical properties of InAs nanowires. *Nano Letters*, *11*, 2424–2429.
- Thelander, C., Dick, K. A., Borgstrom, M. T., Froberg, L. E., Caroff, P., Nilsson, H. A., et al. (2010). The electrical and structural properties of n-type InAs nanowires grown from metal-organic precursors. *Nanotechnology*, *21*, 205703.
- Thelander, C., Frobergfroberg, L. E., Rehnstedt, C., Samuelson, L., & Wernersson, L. E. (2008). Vertical enhancement-mode InAs nanowire field-effect transistor with 50-nm wrap gate. *Electron Device Letters, IEEE*, *29*, 206–208.
- Thelander, C., Mårtensson, T., Björk, M. T., Ohlsson, B. J., Larsson, M. W., Wallenberg, L. R., et al. (2003). Single-electron transistors in heterostructure nanowires. *Applied Physics Letters*, *83*, 2052–2054.
- Theuerer, H. C. (1961). Epitaxial silicon films by the hydrogen reduction of SiCl₄. *Journal of The Electrochemical Society*, *108*, 649–653.
- Thunich, S., Prectel, L., Spirkoska, D., Abstreiter, G., Morral, A., & Holleitner, A. W. (2009). Photocurrent and photoconductance properties of a GaAs nanowire. *Applied Physics Letters*, *95*, 083111.
- Tilburg, J. W. W. V., Algra, R. E., Immink, W. G. G., Verheijen, M., Bakkers, E. P. A. M., & Kouwenhoven, L. P. (2010). Surface passivated InAs/InP core/shell nanowires. *Semiconductor Science and Technology*, *25*, 024011.
- Tomioka, K., & Fukui, T. (2011). Tunnel field-effect transistor using InAs nanowire/Si heterojunction. *Applied Physics Letters*, *98*, 083114.
- Tomioka, K., Motohisa, J., Hara, S., & Fukui, T. (2007). Crystallographic structure of InAs nanowires studied by transmission electron microscopy. *Japanese Journal of Applied Physics*, *46*, L1102–L1104.
- Tomioka, K., Motohisa, J., Hara, S., & Fukui, T. (2008). Control of InAs nanowire growth directions on Si. *Nano Letters*, *8*, 3475–3480.
- Tomioka, K., Motohisa, J., Hara, S., Hiruma, K., & Fukui, T. (2010). GaAs/AlGaAs core multishell nanowire-based light-emitting diodes on Si. *Nano Letters*, *10*, 1639–1644.
- Tomioka, K., Tanaka, T., Hara, S., Hiruma, K., & Fukui, T. (2011). III-V nanowires on Si substrate: selective-area growth and device applications. *Selected Topics in Quantum Electronics, IEEE Journal of*, *17*, 1112–1129.
- Tomioka, K., Yoshimura, M., & Fukui, T. (2011). Vertical In_{0.7}Ga_{0.3}As nanowire surrounding-gate transistors with high-k gate dielectric on Si substrate. In *Electron devices meeting (IEDM), 2011 IEEE international, 5–7 December 2011* (pp. 33.3.1–33.3.4).
- Tomioka, K., Yoshimura, M., & Fukui, T. (2012a). A III-V nanowire channel on silicon for high-performance vertical transistors. *Nature*, *488*, 189–192.

- Tomioka, K., Yoshimura, M., & Fukui, T. (2012b). Steep-slope tunnel field-effect transistors using III-V nanowire/Si heterojunction. VLSI technology (VLSIT). In *2012 Symposium on, 12–14 June 2012* (pp. 47–48).
- Tomioka, K., Yoshimura, M., & Fukui, T. (2013). Sub 60 mV/decade switch using an InAs nanowire–Si heterojunction and turn-on voltage shift with a pulsed doping technique. *Nano Letters*, *13*, 5822–5826.
- Treu, J., Bormann, M., Schmeiduch, H., Döblinger, M., Morkötter, S., Matich, S., et al. (2013). Enhanced luminescence properties of InAs–InAsP core–shell nanowires. *Nano Letters*, *13*, 6070–6077.
- Vaddiraju, S., Sunkara, M. K., Chin, A. H., Ning, C. Z., Dholakia, G. R., & Meyyappan, M. (2007). Synthesis of group III antimonide nanowires. *The Journal of Physical Chemistry C*, *111*, 7339–7347.
- Verheijen, M. A., Immink, G., De Smet, T., Borgström, M. T., & Bakkers, E. P. A. M. (2006). Growth kinetics of heterostructured GaP–GaAs nanowires. *Journal of the American Chemical Society*, *128*, 1353–1359.
- Veuhoff, E., Pletschen, W., Balk, P., & Lüth, H. (1981). Metalorganic CVD of GaAs in a molecular beam system. *Journal of Crystal Growth*, *55*, 30–34.
- Vogel, A. T., Boor, J. D., Becker, M., Wittemann, J. V., Mensah, S. L., Werner, P., et al. (2011). Ag-assisted CBE growth of ordered InSb nanowire arrays. *Nanotechnology*, *22*, 015605.
- Vogel, A. T., De Boor, J., Wittemann, J. V., Mensah, S. L., Werner, P., & Schmidt, V. (2011). Fabrication of high-quality InSb nanowire arrays by chemical beam epitaxy. *Crystal Growth & Design*, *11*, 1896–1900.
- Vurgaftman, I., Meyer, J. R., & Ram-Mohan, L. R. (2001). Band parameters for III–V compound semiconductors and their alloys. *Journal of Applied Physics*, *89*, 5815–5875.
- Wacaser, B. A., Deppert, K., Karlsson, L. S., Samuelson, L., & Seifert, W. (2006). Growth and characterization of defect free GaAs nanowires. *Journal of Crystal Growth*, *287*, 504–508.
- Wagner, R. S., & Ellis, W. C. (1964). Vapor-liquid-solid mechanism of single crystal growth. *Applied Physics Letters*, *4*, 89.
- Wallentin, J., Persson, J. M., Wagner, J. B., Samuelson, L., Deppert, K., & Borgström, M. T. (2010). High-performance single nanowire tunnel diodes. *Nano Letters*, *10*, 974–979.
- Wang, H. (2013). High gain single GaAs nanowire photodetector. *Applied Physics Letters*, *103*, 093101.
- Wang, J., Gudiksen, M. S., Duan, X., Cui, Y., & Lieber, C. M. (2001). Highly polarized photoluminescence and photodetection from single indium phosphide nanowires. *Science*, *293*, 1455–1457.
- Wang, Z., Li, J., Gao, F., & Weber, W. J. (2010). Defects in gallium nitride nanowires: first principles calculations. *Journal of Applied Physics*, *108*, 044305.
- Wang, F., Reece, P. J., Paiman, S., Gao, Q., Tan, H. H., & Jagadish, C. (2011). Nonlinear optical processes in optically trapped InP nanowires. *Nano Letters*, *11*, 4149–4153.
- Wei, W., Bao, X.-Y., Soci, C., Ding, Y., Wang, Z.-L., & Wang, D. (2009). Direct heteroepitaxy of vertical InAs nanowires on Si substrates for broad band photovoltaics and photo-detection. *Nano Letters*, *9*, 2926–2934.
- Welser, J., Hoyt, J. L., Takagi, S., & Gibbons, J. F. (1994). Strain dependence of the performance enhancement in strained-Si n-MOSFETs. *International Electron Devices Meeting (IEDM), Technical Digest*, 373–376.
- Wilhelm, C., Larrue, A., Dai, X., Migas, D., & Soci, C. (2012). Anisotropic photonic properties of III-V nanowires in the zinc-blende and wurtzite phase. *Nanoscale*, *4*, 1446–1454.

- Wilk, G. D., Wallace, R. M., & Anthony, J. M. (2001). High- κ gate dielectrics: current status and materials properties considerations. *Journal of Applied Physics*, *89*, 5243.
- Wu, P. M., Anttu, N., Xu, H. Q., Samuelson, L., & Pistol, M.-E. (2012). Colorful InAs nanowire arrays: from strong to weak absorption with geometrical tuning. *Nano Letters*, *12*, 1990–1995.
- Wu, Z. H., Mei, X., Kim, D., Blumin, M., Ruda, H. E., Liu, J. Q., et al. (2003). Growth, branching, and kinking of molecular-beam epitaxial $\langle 110 \rangle$ GaAs nanowires. *Applied Physics Letters*, *83*, 3368–3370.
- Wu, Z., Neaton, J. B., & Grossman, J. C. (2008). Quantum confinement and electronic properties of tapered silicon nanowires. *Physical Review Letters*, *100*, 246804.
- Wunnicke, O. (2006). Gate capacitance of back-gated nanowire field-effect transistors. *Applied Physics Letters*, *89*, 083102.
- Xiong, Q., Wang, J., & Eklund, P. C. (2006). Coherent twinning phenomena: towards twinning superlattices in III–V semiconducting nanowires. *Nano Letters*, *6*, 2736–2742.
- Xu, T., Dick, K. A., Plissard, S., Nguyen, T. H., Makoudi, Y., Berthe, M., et al. (2012). Faceting, composition and crystal phase evolution in III-V antimonide nanowire heterostructures revealed by combining microscopy techniques. *Nanotechnology*, *23*, 095702.
- Yan, R., Gargas, D., & Yang, P. (2009). Nanowire photonics. *Nature Photonics*, *3*, 569–576.
- Yang, Z. X., Han, N., Wang, F., Cheung, H. Y., Shi, X., Yip, S., et al. (2013). Carbon doping of InSb nanowires for high-performance p-channel field-effect-transistors. *Nanoscale*, *5*, 9671–9676.
- Yang, L., Motohisa, J., Fukui, T., Jia, L. X., Zhang, L., Geng, M. M., et al. (2009). Fabry-Pérot microcavity modes observed in the micro-photoluminescence spectra of the single nanowire with InGaAs/GaAs heterostructure. *Optics Express*, *17*, 9337–9346.
- Zanolli, Z., Fuchs, F., Furthmüller, J., Von Barth, U., & Bechstedt, F. (2007). Model GW band structure of InAs and GaAs in the wurtzite phase. *Physical Review B*, *75*, 245121.
- Zhang, R. Q., Lifshitz, Y., & Lee, S. T. (2003). Oxide-assisted growth of semiconducting nanowires. *Advanced Materials*, *15*, 635–640.
- Zhang, Y., & Loncar, M. (2008). Ultra-high quality factor optical resonators based on semiconductor nanowires. *Optics Express*, *16*, 17400–17409.
- Zhang, G., Tateno, K., Sanada, H., Tawara, T., Gotoh, H., & Nakano, H. (2009). Synthesis of GaAs nanowires with very small diameters and their optical properties with the radial quantum-confinement effect. *Applied Physics Letters*, *95*, 123104.
- Zhang, G., Tateno, K., Suzuki, S., Gotoh, H., & Sogawa, T. (2011). Predominant Si doping through Au catalyst particles in the vapor–liquid–solid mode over the shell layer via the vapor-phase epitaxy mode of InAs nanowires. *The Journal of Physical Chemistry C*, *115*, 2923–2930.
- Zhang, X., Zou, J., Paladugu, M., Guo, Y., Wang, Y., Kim, Y., et al. (2009). Evolution of epitaxial InAs nanowires on GaAs (111)B. *Small*, *5*, 366–369.
- Zollner, S., Garriga, M., Kircher, J., Humlíček, J., Cardona, M., & Neuhold, G. (1993). Temperature dependence of the dielectric function and the interband critical-point parameters of GaP. *Physical Review B*, *48*, 7915–7929.
- Zwiller, V., Akopian, N., Van Weert, M., Van Kouwen, M., Perinetti, U., Kouwenhoven, L., et al. (2008). Optics with single nanowires. *Comptes Rendus Physique*, *9*, 804–815.